Phycologia
2023, Volume 62, Issue 1, Pages 48-67
https://doi.org/10.1080/00318884.2022.2140548
https://archimer.ifremer.fr/doc/00813/92502/

Gonyaulax geomunensis sp. nov. and two allied species (Gonyaulacales, Dinophyceae) from Korean coastal waters and East China Sea: morphology, phylogeny and growth response to changes in temperature and salinity

Kim Hyun Jung [1], Li Zhun [2], Gu Haifeng [3], Mertens Kenneth [4], Yeon Youn Joo [1], Yoon Kwak Kyeong [1], Oh Seok-Jin [5], Shin Kyoungsoon [6], Yoo Yeong Du [7], Lee Wonchoel [8], Shin Hyeon Ho [1, *]

[1] Library of Marine Samples, Korea Institute of Ocean Science & Technology, Geoje, Republic of Korea
[2] Biological Resource Center/Korean Collection for Type Cultures (KCTC), Korea Research Institute of Bioscience and Biotechnology, Jeongeup, Republic of Korea
[3] Department of Marine Biodiversity, Third Institute of Oceanography, Ministry of Natural Resources, Xiamen 361005, China
[4] Ifremer, LITTORAL, Concarneau, France
[5] Laboratory of Coastal Environment and Ecology, Pukyong National University, Busan 48513, Republic of Korea
[6] Ballast Water Research Center, Korea Institute of Ocean Science & Technology, Geoje, Republic of Korea
[7] Faculty of Marine Applied Biosciences, Kunsan National University, Gunsan, Republic of Korea
[8] Department of Life Science, Hanyang University, 222 Wangsipriro, Seongdonggu, Seoul, Republic of Korea

* Corresponding author : Hyeon Ho Shin, email address : shh961121@kiost.ac.kr

Abstract :

Six strains of three different Gonyaulax species were established by isolating cells from the Korean coastal area and the East China Sea, and their morphologies and molecular phylogenies based on SSU and LSU rRNA gene sequences were examined. In addition, the growth responses of the Gonyaulax species to changes in temperature and salinity were investigated. Based on morphological features and phylogenetic positions, Gonyaulax whaseongensis and G. polygramma were identified, and G. geomunensis sp. nov. is proposed in this study. These species displayed the plate formula typical for Gonyaulax, but G. polygramma and G. geomunensis sometimes showed a small intercalary plate (1a) surrounded by plates 2', *3' and 3''. G. geomunensis was morphologically characterized by an S-type ventral organization, descending with a displacement of one cingulum width and bearing one, two or three prominent antapical spines of similar size. The cell surface, which was distinct from other Gonyaulax species, was thick and heavily reticulated into numerous polygonal areas. The reticulation was deeply excavated. The phylogenetics revealed that G. geomunensis and G. whaseongensis belong to different clades, and that there are two ribotypes of G. polygramma, which were morphologically indistinguishable. These species had a close phylogenetic relationship to G. hyalina, and all of them were characterized by dextral torsion. G. whaseongensis, G. polygramma and G. geomunensis had different growth responses

to changes of temperature and salinity, respectively, indicating that morphological and phylogenetic identification of Gonyaulax species can be supported by ecological niches.

Keywords : Cell surface, Gonyaulax fragilis, Growth, Intercalary plate, Ribotype

INTRODUCTION

The genus *Gonyaulax* Diesing was originally described with *Gonyaulax spinifera* (Claparède & J. Lachmann) Diesing as the type species (Diesing 1866; Lewis *et al.* 1999; Carbonell-Moore & Mertens 2019). Thecal plates of *Gonyaulax* species are thick and often heavily reticulated, and the tabulation has been interpreted as 2pr, *4′, 6″, 6C, 5-6s, *5‴, 2p, 1⁗, based on a modified Kofoidian system proposed by Carbonell-Moore *et al.* (2022). Since the first description of *Gonayulax*, more than 120 *Gonyaulax* species have been identified, but several of these have been transferred to other genera (e.g. Sournia 1984; Dodge 1989; Hansen *et al.* 1996; Zhang *et al.* 2020). Currently, 77 species are recognized to belong to *Gonyaulax*, based on some morphological features such as the cingular displacement and overhang, the shape of the sixth precingular plate, the plate ornamentation, the body size and shape, and number and size of antapical spines (e.g. Dodge 1989; Gómez 2012; Mertens *et al*. 2015; Lim *et al*. 2018; Gu *et al*. 2021). In particular, differences in plate ornamentation and cell size were considered important for the identification of *Gonyaulax* species (e.g. Carbonell-Moore & Mertens 2019).

As it is quite difficult to distinguish the thecate stages of different *Gonyaulax* species, the cyst stages, which morphologically resemble fossil-based genera such as *Spiniferites* Mantell, *Impagidinium* Stover & Evitt and *Nematosphaeropsis* Deflandre & Cookson, are useful for the classification of the Gonyaulacales (Ellegaard *et al*. 2002; Mertens *et al*. 2017; Zhang *et al*. 2020; Gu *et al*. 2021, 2022). Nevertheless, in Korean coastal waters some *Gonyaulax* species have been reported by ecologists without detailed morphological and phylogenetic data, leading to confusion over the identity of such species. Recently, a new species, *G. whaseongensis* A.S. Lim, H.J. Jeong & Ji Hye Kim, was described from Korean waters (Lim *et al*. 2018). However, morphological comparisons among *Gonyaulax* species occurring in this area are still insufficient.

Gonyaulax species can be widespread, and occurrences have been recorded in marine, brackish and freshwater environments (Dodge 1989; Lemmermann 1903; Kofoid 1911; Schiller 1937; Andreis *et al*. 1982; Lewis *et al*. 2001; Ellegaard *et al*. 2002, 2003; Mertens *et al*. 2017; Lim *et al*. 2018; Gu *et al*. 2021). In some coastal areas, several *Gonyaulax* species that have been identified as *Gonyaulax spinifera*, *G. membranacea* (M. Rossignol) Ellegaard, Daugbjerg, Rochon, Jane Lewis & I. Harding, and *G. taylorii* Carbonell-Moore have been confirmed as the producers of yessotoxins (YTXs) (Rhodes *et al.* 2006; Riccardi *et al.* 2009; Álvarez *et al.* 2016; Chikwililwa *et al.* 2019; Pitcher *et al.* 2019). Dense blooms of *G. fragilis* (F. Schütt) Kofoid and *G. polygramma* F. Stein have also been reported, and have caused large-scale fish mortalities (Grindley *et al*. 1964; Barwani 1976; Koizumi *et al*. 1996; Al Gheilani *et al*. 2011; van der Lingen *et al*. 2016). However, little is known about the effects of environmental factors such as water temperature and salinity on the growth of *Gonyaulax* species. Water temperature and salinity are the main environmental factors that affect the development of dinoflagellates, and in particular the toxin production and growth of harmful or toxic dinoflagellates (Lee *et al*. 2001; Kim *et al*. 2004; Etheridge & Roesler 2005; Oh *et al*. 2012; Aguilera-Belmonte *et al*. 2013; Han *et al*. 2019). In addition, as many dinoflagellates have different growth responses to changes in water temperature and salinity (Nagasoe *et al*. 2006; Matsubara *et al*. 2007; Xu *et al*. 2010; Jeong *et al*. 2018; Li *et al*. 2021), the implied ecological niches are potentially useful for their classification.

During a study of field samples from Korean coastal areas with the purpose to document the diversity of marine dinoflagellates, small dinoflagellates with heavily reticulated ornamentations were encountered, and six cultures were successfully established. The cultures were examined by light and scanning electron microscopy, and small subunit (SSU) and large subunit (LSU) rDNA sequences were obtained. Based on the results, *G. polygramma* and *G. whaseongensis* were identified, and a new species, *G. geomunensis sp.*

nov. is proposed in this study. In addition, we investigated the growth responses of the identified *Gonyaulax* species to changes in temperature and salinity.

MATERIAL AND METHODS

Sampling and cultures

Plankton samples were collected from the Korean coastal area and the East China Sea using a 20-μm-mesh plankton net (Fig. 1; Table 1). *Gonyaulax* species were isolated immediately on the research vessel or in the laboratory with a capillary pipette, using an Eclipse 50i light microscope (Nikon, Tokyo, Japan). The isolated cells were inoculated into individual wells of 48-well culture plates (Eppendorf, Hamburg, Germany) filled with f/2-Si culture medium (Marine Water Enrichment Solution, Sigma-Aldrich, St. Louis, Missouri, USA) and cultured at 20℃ and *c.* 100 μmol photons m^{-2} s^{-1} cool-white illumination and a 12:12 h light:dark cycle. The cultured cells were transferred to six-well culture plates, and after sufficient growth the cultures were transferred to a 70025 SPL culture flask (SPL Life Science, Pocheon, Korea) containing 25 ml of sterile f/2-Si culture medium. Six culture strains of several *Gonyaulax* species were established successfully and deposited at the Library of Marine Samples, Korea Institute of Ocean Science and Technology, Republic of Korea (Table 1).

Light microscopy (LM)

Living cells of the strains were photographed at ×1000 magnification using an ultra-high resolution DS-Ri2 digital camera (Nikon) on an Eclipse Ni upright microscope (Nikon). Cell size was measured based on LM images. For fluorescence microscopy, approximately 1 ml of culture was transferred to a 1.7-ml microcentrifuge tube, and SYTOX® Green Nucleic Acid

Stain (Molecular Probes, Eugene, Oregon, USA) was added at a final concentration of 1.0 μM. The cells were incubated in the dark at room temperature for 30 min. The cells were observed through a Zeiss Filterset (emission: BP 450–490; beam splitter: FT510) and photographed using an Axio-Cam MRc digital camera on an Axio Imager 2 upright microscope (Zeiss, Oberkochen, Germany).

Scanning electron microscopy (SEM)

For SEM, 2 ml of mid-exponential batch cultures were fixed with Lugol's iodine solution (0.1% final concentration) for 24 h at room temperature, then rinsed with deionized water. After rinsing, the samples were dehydrated in a graded ethanol series (10%–99% in seven steps) for 10 min at each step and then critical point dried using a SPI-Dry Regular Critical Point Dryer (SPI Supplies, West Chester, Pennsylvania, USA) using liquid CO_2. Finally, the samples were coated with platinum and examined under a JEOL JSM 7600F field emission scanning electron microscope (JEOL Ltd, Tokyo, Japan). Plate labelling followed the modified Kofoidian system proposed by Carbonell-Moore *et al*. (2022).

DNA extraction and sequencing

Genomic DNA was extracted from 1 ml of exponentially growing cultures of *Gonyaulax* species using the DNeasy Plant Mini Kit (QIAGEN Inc., Valencia, California, USA) following the manufacturer's instructions. The SSU rRNA gene sequence was amplified using the primer pairs SR1 and SR12b (Takano & Horiguchi 2004), and the partial LSU rRNA gene sequence was amplified using the primer pairs 25F1 and R2 (Yamaguchi & Horiguchi 2005; Takano & Horiguchi 2006). The PCR was conducted using a Thermal Cycler (Mastercycler® nexus, Eppendorf, Hamburg, Germany) at 98℃ for 5 min, followed by 30 cycles of denaturation at 98℃ for 10 s, annealing at 58℃ for 15 s, and extension at 68℃ for 2 min. The reaction was completed with a final elongation at 68℃ for 5 min. The PCR

amplified products were confirmed by 1% agarose gel electrophoresis. The PCR products were purified using the QIAquick PCR Purification Kit (QIAGEN). The cycle sequencing reaction was performed using the ABI PRISM BigDyeTM Terminator v3.1 Cycle Sequencing Ready Reaction Kit (Applied Biosystems, Waltham, Massachusetts, USA).

Sequence alignment and phylogenetic analysis

Sequence alignments were carried out with MAFFT v7.110 (Katoh *et al*. 2019) and the Q-INS-I option to consider rRNA secondary structure. The final alignment of the SSU rDNA dataset consisted of 57 taxa and contained 1,420 characters (including inserted gaps). *Adenoides eludens* (Herdman) Balech (LC002841) was used as the outgroup. For the analysis of LSU rDNA, the dataset contained 73 taxa and consisted of 1,158 characters. *Adenoides eludens* (LC002846) was used as the outgroup. The separate alignments were then checked and concatenated using SequenceMatrix v1.8 (Vaidya *et al.* 2011). For the analysis of SSU–LSU rDNA concatenated sequences, the data set contained 87 taxa and consisted of 3,476 characters (including gaps introduced for alignment). *Adenoides eludens* (LC002841/LC0028464) was used as outgroup to root the trees. The GTR+I+G substitution model was selected using the Akaike information criterion, as implemented in jModelTest v2.1.10 (Darriba *et al*. 2012).

Phylogenetic trees for the datasets were constructed using maximum likelihood (ML) analyses and Bayesian inference (BI). The ML analyses were performed using RAxML v8 (Stamatakis *et al*. 2014). Bootstrap analyses for datasets were carried out using ML with 1,000 replicates to evaluate the statistical reliability. Bayesian inference analyses were conducted of both datasets using the MrBayes program v3.2 (Ronquist *et al*. 2012). Five Markov chain Monte Carlo (MCMC) chains were run for 10 million generations, sampling every 100 generations. The final tree was visualized using MEGA11 (Tamura *et al*. 2021).

Growth experiments

To examine the specific growth rate of the *Gonyaulax* species, a growth experiment was performed under different water temperatures and salinities. Six temperature conditions (5, 10, 15, 20, 25 and 30℃) and six salinities (15, 20, 25, 30, 35 and 40) were combined under a fixed irradiance of *c.* 100 μmol photons m^{-2} s^{-1} cool-white illumination and a 12:12 h light:dark cycle. In the experiment, salinity levels below 30 were obtained by diluting seawater with ultra-distilled water. The subcultures of *Gonyaulax* species for the experiments were established in two-litre culture bottles (SPL Life Science), and these were used for inoculation into experimental tubes; 300 cells of *Gonyaulax* species were inoculated into a 50-ml Pyrex bottle. Growth experiments were conducted in triplicate.

Culture growth was monitored at two-day intervals using an *in vivo* fluorometer (Turner Designs 10-AU, Sunnyvale, California, USA), and the fluorescence data were used to calculate specific growth rates. The regression equation for *in vivo* fluorescence values provided a good fit to the observed cell densities from samples fixed with Lugol's solution; the adjusted r^2 values for *Gonyaulax* species were >0.99 (Fig. S1). To estimate the specific growth rate (μ) of *Gonyaulax*, we used the following equation (Guillard 1973):

$$\mu = \log_2 (N_t - N_0) / t_1 - t_0$$

where N_0 and N_t are the *in vivo* fluorescence values at the initial (t_0) and final (t_1) stages during the incubation experiments, respectively. In this study, the *in vivo* fluorescence values estimated during logarithmic growth phase were used to obtain the specific growth rate. Contour plots of the specific growth rates were generated by the software package Surfer v14 using the maximum curvature gridding method.

RESULTS

Morphology of *Gonyaulax* species from Korean coastal waters and East China Sea

The formal taxonomic description of the new species is at the end of Discussion.

GONYAULAX GEOMUNENSIS SP. NOV.

Cells of this species are illustrated by LM in Figs 2–7, by SEM in Figs 8–23 and by schematic drawings in Figs 24–27. Cells were yellowish and ovoidal with a pronounced apex that was slightly angled to the right (Figs 2, 3). The shoulders were pronounced and the cingulum was descending and displaced (Fig. 2). The cell surface was covered with reticulations, visible in LM (Fig. 4). Cells had a rounded hypotheca with 0–3 short antapical spines (Fig. 6). Some granular contents were visible in dorsal view (Fig. 6). The shape of the marginally distributed chloroplasts was unclear (Fig. 7). The nucleus was subspherical and located in the hypotheca (Figs 5, 7). Cells were 25.5–43.9 μm long (mean = 33.4 μm, n = 30) and 23.4–35.0 wide (mean = 28.5 μm, n = 30). Cell length:width (L:W) ratios were 1.0–1.4 (mean = 1.2, n = 30), and cell epi- to hypotheca (E:H) ratios were 1.0–1.4 (mean = 1.2, n = 16).

Based on SEM observations, the plate formula was Po, *4′, 1a, 6″, 6C, 5S, 5‴, 2p, 1⁗ (Figs 8–23). Observed cells had an S-type ventral organization, and 1–3 prominent antapical spines of similar sizes on the antapical plate (1‴; Figs 8–11, 13, 14), although some cells lacked such spines (Figs 12, 15). The shapes and lengths of antapical spines were variable within the strain. The theca was thick, and heavily reticulated with numerous polygonal depressions (Figs 8–23). The reticulation was deeply excavated and made plate boundaries difficult to observe. A small ventral pore was present at the intersection between plates 1′, *4′a and *4′p (Figs 16–18). The apical pore complex (APC) was smooth and lenticular,

surrounded by raised ridges of the plates 1′, 2′, *4′a and *4′p (Figs 8–11, 17, 18). The *4′a, surrounded by APC and plates 1′, *3′ and *4′p, was small and difficult to distinguish at the boundaries of plates *3′ and *4′p (Figs 8, 16–20). The first apical plate (1′), surrounded by the APC, plates 2′, *4′a, *4′p, 1″ and the anterior sulcal plate (Sa), was narrow and slender, slightly excavated and sigmoid (Figs 8–10, 16–19). Plate *4′p was small and pentagonal (Figs 8, 16–20). Compared to the sizes of plates 1′ and *4′p, plates 2′ and *3′ were large and occupied the dorsal part (Figs 8–11, 20). The precingular plates were quadrangular, large and similar in size except for plate 6″ (Figs 8–11, 20). A very small triangular anterior intercalary plate (1a) was clearly observed in the internal view (Fig. 21), and was located on the dorsal area and surrounded by plates 2′, *3′ and 3″ (Figs 18, 21). The cingulum was deeply excavated, without overhang, and descended with a displacement of more than one cingulum width (about 1.3–1.8 cingulum widths; Figs 8, 9, 19). The cingulum comprised six plates, of which plate C4 was the smallest (Fig. 11).

The sulcal plates comprised the anterior sulcal plate (Sa), anterior left sulcal plate (Ssa) and right sulcal plate (Sda), posterior left sulcal plate (Ssp) and right sulcal plate (Sdp). The Sa contacted with plates 1′, *4′p, 1″, 6″ (Figs 8, 9, 16, 19, 22). There were four postcingular plates, of similar size except for plate *2‴ (Figs 14, 23). In the postcingular, plates *2‴, *4‴, *5‴ and *6‴ were quadrangular, and plate *3‴ was pentagonal (Figs 10–14, 23). The thecae demonstrated dextral torsion (Fig. 11). Plate 1p was quadrangular and surrounded by *2‴, *3‴ and 1⁗ (Figs 8–10, 15), and plate 2p was smooth and extended to the hypotheca (Figs 8, 9, 12, 15, 22). The antapical plate (1⁗) was surrounded by plates *3‴, *4‴, *5‴ and *6‴, and 2p was located in the middle of the hypotheca; a short and curved spine, or two or three short and straight antapical spines, were sometimes observed on the rim of 2p touching 1⁗ (Figs 8, 9, 13–15, 23). The spines were 0.6–2.8 μm in length (mean = 1.8 μm, n = 8).

GONYAULAX WHASEONGENSIS A.S. LIM, H.J. JEONG & JI HYE KIM

Cells of this species are illustrated by LM in Figs 28–33, by SEM in Figs 34–49 and by schematic drawings in Figs 50–53. Based on LM observations, cells were brownish-yellow and ovoidal with a pronounced apex that was slightly angled to the cell's right (toward the left in ventral view; Fig. 28). The cingulum was descending, displaced, and the sulcal area was deeply impressed (Fig. 28). Cells had a conical epitheca and a rounded hypotheca with a prominent left antapical spine (Figs 28–32). The nucleus was spherical and located in the hypotheca (Fig. 33). The chloroplasts were distributed throughout the cell (Fig. 33); their shape was unclear. Cells were 38.6–42.7 μm long (mean = 40.6 μm, n = 15) and 31.7–33.4 wide (mean = 32.7 μm, n = 15).

The plate formula was Po, *4′, 6″, 6C, 5S, 5‴, 2p, 1⁗, with an S-type ventral organization and one or two antapical spines (Figs 34–39). The left antapical spine was prominent, and straight or curved (Figs 34, 38, 39). The shapes and lengths of the antapical spines were variable within the strain. The cell surface was thick and reticulated, with many randomly scattered small pores (Fig. 40). The reticulation of the theca was shallow and the plate boundaries were distinct. A ventral pore was present on the intersection between *4′a and *4′p (Figs 41, 42). The APC was smooth and lenticular, surrounded by raised ridges of plates 2′ and *4′a (Figs 43, 44). Plate *4′a contacted plates 2′, *4′ and *4′p (Fig. 43). Plate 1′ was narrow, slightly curved, and contacted 1″ (Figs 39, 41–44). A row of small pores was visible at the right margin of plate 1′ (Fig. 45). Plates 2′ and *3′ were of similar size, hexagonal, and occupied the dorsal part (Figs 35–37, 43, 44). Plate *4′p was narrow, hexagonal, elongated and contacted *4′a, *3′, 5″, 6″ and Sa (Figs 34, 41–44). There were six precingular plates, of which 6″ was the smallest, and the others were of similar size (Figs 43, 44). The cingulum was deeply excavated with a slight overhang, and descended with a

displacement of more than one cingulum width (about 1.2–2.0 cingulum widths) (Figs 34, 39, 42). The cingulum comprised six plates (Figs 34–38).

The sulcal area was deeply excavated and partially covered by plates 6″, *2‴, C6 and 1p (Figs 34, 38–40, 42, 46–48), and the sulcal plates comprised Sa, Ssa, Sda, Ssp and Sdp (Figs 46–48). There were four postcingular plates of similar size except for plate *2‴ (Fig. 49). The plate Ssa was small and elongated (Figs 34, 38–40, 46). Plates *3‴, *4‴, *5‴ and *6‴ were quadrangular (Figs 34–37, 49). The thecae displayed dextral torsion (Fig. 36). Plate 1p was narrow and elongated, and was sometimes divided into two plates, $1p^a$ and $1p^b$ (Fig. S2), and contacted plates *2‴, *3‴ and 1‴″ (Figs 34, 38–40, 49). Surface of plate 2p was smooth, but pores were visible on the 2p plate (Figs 38, 39, 48). Plate 1‴″ was surrounded by *2‴, *3‴, *4‴, *5‴, *6‴ and 2p (Fig. 49). A short spine and a long, thick and sharply pointed spine were present on rim of 1‴″ touching 2p (Figs 38–40, 49), and in antapical view the spines sometimes seemed to have wide bases surrounding the 2p (Fig. 49). A long spine was 2.1–6.0 μm in length (mean = 4.3 μm, n = 12).

GONYAULAX POLYGRAMMA F. STEIN

Two ribotypes, *G. polygramma* ribotype 1 and 2, were identified in the molecular phylogenies. However, there were no critical differences in the morphologies of the two ribotypes, except for a difference in cingular displacement. Cells of ribotype 1 are illustrated by LM in Figs 54–59, by SEM in Figs 66–78 and by schematic drawings in Figs 91, 92, 95, 96. *Gonyaulax polygramma* ribotype 2 is illustrated by LM in Figs 60–65, by SEM in Figs 79–90 and by schematic drawings in Figs 93, 94, 97, 98.

Cells of *G. polygramma* were yellowish and slightly elongated (Figs 54–58, 60–64). A pronounced angled apex and shoulders in the epitheca, and a prominent, curved, left antapical spine in the hypotheca were clearly visible in LM (Figs 55, 60). The shapes and lengths of the antapical spines were variable within each strain. A subspherical nucleus was located in the

hypotheca, and the marginally distributed chloroplasts had an unclear shape (Figs 59, 65). Cells of *G. polygramma* ribotype 1 were 33.2–44.5 μm long (mean = 38.5 μm, n = 32) and 27.6–36.8 wide (mean = 31.0 μm, n = 32); and cells of *G. polygramma* ribotype 2 were 32.1–47.9 μm long (mean = 36.9 μm, n = 30) and 24.5–37.2 wide (mean = 29.6 μm, n = 30).

The plate formula was Po, 4′, (1a), 6″, 6C, 5S, 5‴, 2p, 1⁗, and there was an S-type ventral organization (Figs 66, 79). Thecal plates were reticulated with numerous randomly distributed but also some regularly arranged pores. Sometimes somewhat shallow reticulations were visible. Well-developed longitudinal ridges in the epitheca were distinct from those of the hypotheca, and were parallel to plate boundaries. A ventral pore was present on the intersection between 1′, *4′a and *4′p (Figs 66, 70–72, 79, 83, 84). The APC, surrounded by raised ridges of 1′, 2′, 3′ and *4′a, was smooth and lenticular (Figs 75, 87). Plate *4′a contacted the left margin of plate *3′ (Figs 72–75, 83–87). Plate 1′ was very long and narrow, touched the APC and was hidden by 2′ and *4′a (Figs 66, 67, 71, 72, 79, 83, 84, 87). Plates 2′ and *3′ were of similar size and occupied the dorsal part (Figs 69, 73, 75, 81, 85, 87). Plate *4′p was small, nearly pentagonal and contacted *3′, *4′a, 5″, 6″ and Sa (Figs 66, 70–72, 79, 82–84). A small plate 1a was sometimes observed, surrounded by plate 2′, *3′ and 3″ (Figs 73, 75, 81, 85, 86), but was absent from some cells (Figs 69, 74, 87). There were six precingular plates, which were tetragonal (Figs 75, 87). The cingulum was deeply excavated, with a slight overhang, and descended with a displacement of more than one cingulum width (about 1.7–2.1 cingulum widths in *G. polygramma* ribotype 1 and 1.3–1.4 cingulum widths in *G. polygramma* ribotype 2). The cingulum comprised six plates (Figs 66–71, 79–82, 86).

The sulcal area was deeply excavated. Plate Sa touched plates 1′, *4′p, 1″ and 6″, and was narrow and long (Figs 66, 67, 70–72, 76, 79, 82–84, 88, 89). In the postcingular plate series, the Ssa plate was smallest, and other plates were similar in size and quadrangular in

shape (Figs 66, 67, 70–72, 76, 77, 79, 82–84, 88, 89). The thecae displayed dextral torsion (Figs 68, 69, 81, 86). Plate 1p was surrounded by 2p, *2‴, *3‴ and 1‴′, and 1p was long, narrow and elongated (Figs 66, 67, 70, 76, 77, 79, 80, 88, 89). Plate 2p was smooth, without a reticulated ornamentation but provided with pores (Figs 66, 67, 76, 77, 79, 88, 89). Plate 1‴′ was surrounded by 1p, 2p, *3‴, *4‴, *5‴ and *6‴ (Figs 78, 90). Two to four minute spines, and a long and straight spine were present on the rim of 2p touching 1p and 1‴′ (Figs 66–71, 76, 78–80, 82, 88, 90), but the minute spines were not observed under LM. The long spine was 0.8–6.3 μm in length (mean 3.8, n = 32).

Molecular phylogeny of *Gonyaulax* species from Korean coastal waters and East China Sea

The phylogenetic tree inferred from the concatenation of the SSU–LSU sequences is shown in Fig. 99. The ML tree based on the concatenated sequences showed four well-resolved clades, corresponding to families Gonyaulacaceae, Ceratiaceae, Protoceratiaceae and Lingulodiniaceae. The family Gonyaulacaceae included the cyst-based genera *Spiniferites*, *Impagidinium*, *Bitectatodinium* G.J. Wilson, *Ataxiodinium* P.C. Reid and *Tectatodinium* D. Wall. *Gonyaulax geomunensis* was clearly divergent from other *Gonyaulax* species in the family Gonyaulacaceae, and appeared as sister to *G. hyalina* Ostenfeld & E.J. Schmidt, with moderate support (ML bootstrap support 92, BI posterior probability 0.93). Our isolate of *G. whaseongensis* (accessions OM692365/OM729601) shared an identical sequence with previously studied Korean strains of *G. whaseongensis* (accession LS481152) and Chinese isolates of *Spiniferites hyperacanthus* (Deflandre & Cookson) Cookson & Eisenack. Of the two ribotypes identified for Korean strains of *G. polygramma*, strains LIMS-PS-3466 and LIMS-PS-3467 (accessions OM692366/OM729602 and OM692367/OM729603) are nested within ribotype 1 (ML 98, BI 1.0), whereas the ribotype 2 includes strains LIMS-PS-3346 and LIMS-PS-3347 (accessions OM692368/OM729604 and OM692369/OM729605) (ML

99, BI 1.0). The larger clade, consisting of isolates of *G. whaseongensis*, *G. geomunensis*, *G. hyalina*, *G. polygramma*, *Tectatodinium pellitum* D. Wall and *Ataxiodinium choanum* P.C. Reid were clearly divergent from other *Gonyaulax* species such as *G. digitale* (C.H.G. Pouchet) Kofoid, *G. spinifera*, *G. membranacea* and *G. ellegaardiae* K.N. Mertens, H. Aydin, Y. Takano, A. Yamaguchi et Matsuoka.

The individual gene trees (SSU and LSU rDNA) resulted in patterns similar to those observed from the multiple genes trees (Figs S3, S4). In a phylogenetic tree based on the SSU rRNA gene sequence, the family Gonyaulacaceae was monophyletic comprising *Gonyaulax* species and several cyst-based genera with strong support (ML 99, BI 1.0). *Gonyaulax geomunensis* formed a sister clade to *G. hyalina*, although with weak support (ML 51, BI 0.84). *Gonyaulax whaseongensis* and *S. hyperacanthus* grouped together with maximum support, and *G. polygramma* displayed the two ribotypes. The LSU rRNA gene tree showed a larger clade consisting of isolates of *G. whaseongensis*, *G. geomunensis*, *G. hyalina*, *G. polygramma*, *Tectatodinium pellitum*, and *Ataxiodinium choanum*, which were divergent from other *Gonyaulax* species. Within this clade, *G. geomunensis* appeared as sister to *G. hyalina*, with weak support (ML 66, BI 0.83). Korean isolates of *G. whaseongensis* grouped together with Chinese isolates of *S. hyperacanthus* with high support. The two ribotypes of *G. polygramma* were identified, with strong support (ML 99, BI 1.0).

Growth responses of *Gonyaulax* species to changes in combinations of temperature and salinity

The growth rates of *Gonyaulax geomunensis*, *G. whaseongensis* and *G. polygramma* ribotypes 1 and 2 exposed to combinations of temperatures and salinity conditions are shown in Figs 100–103 and Table S1. Linear relationships between cell concentrations and *in vivo* fluorescence for tested *Gonyaulax* species are provided in Fig. S1.

Growth of *G. geomunensis* was only observed at 25℃ and salinities of 25 and 30. The maximum growth rate was 0.39 d^{-1}, obtained at 25℃ and salinity of 30. At 25℃ and salinity of 25, the growth rate was 0.28 d^{-1} (Figs 100, S5; Table S1). In contrast with *G. geomunensis*, the growth of *G. whaseongensis,* and *G. polygramma* ribotypes 1 and 2 were observed under a wide range of combinations of temperatures and salinities. The growth rate of *G. whaseongensis* ranged from 0.0 to 0.48 d^{-1}, and the highest growth rate was observed at 30℃ and salinity of 30. At 15℃, no growth of *G. whaseongensis* occurred at salinities of 15 and 20 (Figs 101, S6; Table S1). At temperatures above 20℃, *G. whaseongensis* could grow at all tested salinities, and higher growth rates were observed with increasing salinity level until salinity 40, at which the growth rates decreased at all tested temperatures.

The growth responses of *G. polygramma* ribotypes 1 and 2 to combinations of temperature and salinity were similar, but at almost all tested conditions of temperature and salinity the growth rates were higher for *G. polygramma* ribotype 1 than for ribotype 2. The highest growth rates of both ribotypes were observed at 25℃ (0.24 d^{-1} for ribotype 1 and 0.18 d^{-1} for ribotype 2; Figs 102, 103, S7, S8; Table S1). Relatively high growth rates of *G. polygramma* ribotype 1 were observed at 20℃ and 25℃, and salinity of 25 and 30. At salinities of 15 and 20, *G. polygramma* ribotype 2 could not grow at all tested temperatures, but *G. polygramma* ribotype 1 grew at salinity 20 at temperatures 20℃ and 25℃.

DISCUSSION

Cell size and cingular width of *Gonyaulax whaseongensis*, *G. geomunensis* and *G. polygramma*

Most records of *Gonyaulax* species from Korean coastal waters published in ecological surveys lack detailed morphological and phylogenetic information. More accurate taxonomical studies are needed to reliably identify the *Gonyaulax* species present in the

region. Morphological comparisons, based on LM and SEM, of *Gonyaulax whaseongensis*, *G. polygramma* and *G. geomunensis* collected from Korean coastal area and East China Sea are provided in Table 2.

Gonyaulax geomunensis, *G. whaseongensis* and *G. polygramma* share the presence of a ventral pore, dextral torsion, small displacement of the cingulum, slight overhang, similar shape and location of nucleus, and similar shape of each thecal plate. However, the cell size and the L:W ratio of *G. geomunensis* are smaller than those of *G. whaseongensis* and *G. polygramma*; the L:W ratio of *G. geomunensis* was 1.1, whereas L:W ratios of *G. whaseongensis* and two ribotypes of *G. polygramma* were 1.2, 1.2 and 1.3, respectively. *Gonyaulax geomunensis* was also smaller than *G. baltica* Ellegaard, Jane Lewis & I. Harding (mean = 35.8 μm long), *G. diegensis* (75–100 μm long), *G. digitale* (40–63 μm long), *G. ellegaardiae* (30.5–43.4 μm long), *G. elongata* (P.C. Reid) Ellegaard, Daugbjerg, Rochon, Jane Lewis & I. Harding (mean = 36 μm long), *G. membranacea* (mean = 34 μm long) and *G. spinifera* (44–64 μm long) (Kofoid 1911; Dodge 1989; Lewis *et al*. 2001; Ellegaard *et al*. 2002, 2003; Riccardi *et al*. 2009; Mertens *et al*. 2015, 2017). However, as was often reported, cell sizes of *Gonyaulax* species varied among specimens, and the use of cell sizes to identify *Gonyaulax* species should be treated with caution (e.g. Carbonell-Moore & Mertens 2019).

Recently, *G. whaseongensis* from Korean coastal waters was described as a new *Gonyaulax* species by Lim *et al*. (2018). According to Lim *et al*. (2018), *G. whaseongensis* is morphologically distinguished from other *Gonyaulax* species by the narrow cingulum (*c.* 2.6 μm wide), the small cingular displacement, the slight overhang and the steep angle between the cingular ends, the shape of the sixth precingular plate, and the number and shape of antapical spines. However, the cingular width of our isolates of *G. whaseongensis* is slightly larger (2.9 μm) than in specimens described by Lim *et al*. (2018). In addition, in the present study there was little difference even in the cingular width between ribotypes of *G.*

polygramma. Although some taxonomical studies included the cingular displacements and overhangs for the identification of *Gonyaulax* species (Kofoid 1911; Ellegaard *et al*. 2003; Mertens *et al*. 2015; Lim *et al*. 2018), these morphological features do not seem to be very useful to differentiate the present group of species.

Surface ornamentation of *Gonyaulax whaseongensis*, *G. geomunensis* and *G. polygramma*

The surface ornamentation of many *Gonyaulax* species usually includes reticulations with raised ridges (Kofoid 1911; Andreis 1982; Ellegaard *et al*. 2003: Gu *et al*. 2021), and the differences in reticulations or ornamentation are important to identify *Gonyaulax* species (Carbonell-Moore & Mertens 2019). In particular, the surface ornamentation of *Gonyaulax polygramma*, which is characterized by well-developed longitudinal ridges in thecal plates, differs clearly from those of *G. whaseongensis*, *G. geomunensis* and other *Gonyaulax* species (Stein 1883; Lemmermann 1903; Kofoid 1911; Lebour 1925; Schiller 1937; Andreis 1982; Balech 1988; Dodge 1988; Kang *et al*. 2018; Lim *et al*. 2018; Gu *et al*. 2021).

The cell surface of *G. geomunensis* is heavily reticulated with numerous polygonal depressions, and the reticulation is deeply excavated, which is quite similar to that of *Sourniaea diacantha* (Meunier) H. Gu, K.N. Mertens, Zhun Li & H.H. Shin (see fig. 13 in Zhang *et al*. 2020), which had previously been identified as *G. verior* Sournia. The reticulation affords distinction of *G. geomunensis* from *G. whaseongensis* and *G. polygramma*, as well as from *G. hyalina* and *G. fragilis* (Carbonell-Moore & Mertens 2019). Based on SEM observations, similar cell surfaces were also reported in some motile cells germinated from *Spiniferites* cysts (Gu *et al*. 2021); however, the reticulations seemed to be somewhat shallower than those of *G. geomunensis*.

In specimens of *G. whaseongensis* shown in this study and the publication by Lim *et al.* (2018), this species has many randomly scattered small pores, and in particular, a row of

small pores on the plate 1′, which is not observed in other *Gonyaulax* species, including *G. geomunsensis* and *G. polygramma* (see fig. 2b in Lim *et al*. 2018; Fig. 45). These small pores are also observed in the motile cell germinated from *Spiniferites hyperacanthus* that shares identical sequences with *G. whaseongensis* (Gu *et al*. 2021). This indicates that the presence of small pores on 1′ can be one of the features for distinguishing *G. whaseongensis* from other *Gonyaulax* species. However, as the row of small pores on plate 1′ is frequently hidden by plate *4′p, it is difficult to observe, requiring examination by SEM.

Small anterior intercalary plate of *G. geomunensis* and *G. polygramma*

In our isolates of *G. polygramma*, the small anterior intercalary plate (1a), which had not been described previously, was observed on the dorsal part of the theca, although it was not visible in all thecae. *Gonyaulax geomunensis* also has plate 1a surrounded by plates 2′, *3′ and 3″. The presence of a plate 1a has previously been recorded in *G. hyalina* and *G. fragilis* (Escalera *et al*. 2018; Carbonell-Moore & Mertens 2019), and Escalera *et al*. (2018) recorded that the presence of plate 1a (described as a very small triangular platelet on the dorsal portion of the suture between 4′a and 2′) was very variable even within the same strain. Interestingly, plate 1a was reported only in *G. polygramma* and *G. hyalina*, both of which are closely related to *G. geomunensis*.

The discovery of an anterior intercalary plate in these extant species is reminiscent of the anterior intercalary plates recorded for Mesozoic gonyaulacalean genera, first documented by Stover & Evitt (1978, pp 275–279). This seems to be a case of atavism, and another was recently discovered by Kretschmann *et al*. (2022). Given that *G. fragilis* and *G. hyalina* belong to the subgenus *Steiniella* (Escalera *et al*. 2018; Carbonell-Moore & Mertens 2019), this genus might need to be re-erected to encompass these species with a potential

presence of an anterior intercalary plate. This also seems to correspond to their phylogenetic placement (see below).

Antapical spines of *Gonyaulax whaseongensis*, *G. geomunensis* and *G. polygramma*

Gonyaulax whaseongensis, G. geomunensis and *G. polygramma* show differences in the shape of the antapical spines. In ventral view *G. whaseongensis* shows a short and sharply pointed spine, which is sometimes visible as a collar-like shape in antapical view, and a long and sharply pointed spine on the rim of 1′′′′ touching 2p (Fig. 39). In contrast, *G. geomunensis* and *G. polygramma* have narrow, long and straight antapical spines. *Gonyaulax polygramma* can have three or four antapical spines. In addition, the spines of *G. whaseongensis* seem to be slightly longer (4.3 μm) than those of *G. geomunensis* (1.8 μm) and *G. polygramma* (3.8 μm). However, the shapes and length of spines of these species can be variable, even within the same strain. In previous publications, several prominent antapical spines were reported in some *Gonyaulax* species, such as *G. spinifera, G. digitale* (Kofoid 1911), *G. ellegaardiae* (Mertens *et al*. 2015), *G. membranacea*, and *G. elongata* (Ellegaard *et al*. 2003), *G. baltica* (Ellegaard *et al*. 2002; Mertens *et al*. 2017) and unspecified *Gonyaulax* species germinated from *Spiniferites*-like cysts (Gu *et al*. 2021). Of these species, *G. ellegaardiae* shows a flipper-like antapical spine in ventral view (Mertens *et al*. 2015), whereas other *Gonyaulax* species have two short or long antapical spines of similar or unequal size, or have minute spines (Kofoid 1911; Ellegaard *et al*. 2002, 2003; Mertens *et al*. 2017; Gu *et al*. 2021, 2022). Spines may therefore be a useful feature but are often not enough for unambiguously distinguishing many species of *Gonyaulax*. In addition, *G. hyalina* and *G. fragilis* do not have any antapical spines (Carbonell-Moore & Mertens 2019).

Cysts of *Gonyaulax whaseongensis*, *G. geomunensis* and *G. polygramma*

Although many features have been proposed to differentiate *Gonyaulax* species, it is quite difficult to distinguish the thecate stages of different species, as shown in this study. Recently, Gu *et al*. (2021) described cysts resembling *Spiniferites hyperacanthus* from Chinese coastal sediments and recorded that the cells germinated from *S. hyperacanthus* and *G. whaseongensis* have identical SSU and LSU rRNA gene sequences and morphological features. According to Mertens *et al*. (2017) and Gu *et al*. (2021, 2022), the morphologically distinct features of *Spiniferites* species can be useful for identifying *Gonyaulax* species. Unfortunately, we could not observe cysts of *G. geomunensis* and *G. polygramma* in cultures, either because these strains are heterothalic or perhaps because they do not produce sexual resting cysts. However, as Lim *et al*. (2018) also did not observe the cyst of *G. whaseongensis* in their encystment experiment and Taylor (1962, pl. I, fig. 5) suggested a cyst inside a theca of *G. polygramma*, further studies are needed to investigate the cyst-theca relationships of *G. geomunensis* and *G. polygramma*.

Phylogenetic positions

The molecular phylogenetic results clearly showed that *G. whaseongensis* and *G. geomunensis* form a separate clade from other *Gonyaulax species*, and two ribotypes of *G. polygramma* were inferred here for the first time. It is surprising that only Korean sequences of *G. polygramma* are available in GenBank, despite the fact that morphological features of *G. polygramma* have been described from many coastal areas (e.g. Stein 1883; Lemmermann 1903; Kofoid 1911; Lebour 1925; Schiller 1937; Andreis 1982; Balech 1988; Dodge 1988; Kang *et al*. 2018). In our phylogenetic tree, *G. whaseongensis, G. geomunensis, G. hyalina* and *G. polygramma* shared a dextral torsion and are phylogenetically grouped as a larger clade, which is clearly divergent from other *Gonyaulax* species, such as *G. digitale, G.*

spinifera, *G. membranacea* and *G. ellegaardiae*, which have a neutral torsion (Kofoid 1911; Ellegaard *et al*. 2003; Mertens *et al*. 2015).

Despite the reports of dense blooms of *G. polygramma* in many coastal waters of the world (Morton & Villareal 1998; Cho 2005; Kumar *et al*. 2020), available rRNA gene sequences of this species are still limited. In our phylogenetic tree, morphologically indistinguishable Korean isolates of *G. polygramma* comprised two ribotypes, suggesting that *G. polygramma* forms a species complex, with at least two cryptic species. Two ribotypes have been identified in *G. baltica* and other dinoflagellates such as *Margalefidinium polykrikoides* (Margalef) F. Gómez, Richlen & D.M. Anderson (formerly *Cochlodinium polykrikoides* Margalef), *Bysmatrum subsalsum* (Ostenfeld) M.A. Faust & Steidinger and *Sourniaea diacantha*, and the occurrence of each ribotype was related to a particular geographic distribution (Iwataki *et al*. 2008; Zhang *et al*. 2020; Park *et al*. 2021; Gu et al. 2022). According to Li *et al*. (2015) and Park *et al*. (2018), the occurrences of *M. polykrikoides* ribotypes in Korean coastal waters could be attributed to human-assisted dispersal (e.g. ballast waters) and water currents formed in Asian coastal areas. However, how *G. polygramma* was introduced into Korean coastal waters is not currently clear. In addition, as the cingular displacement of *G. polygramma* ribotype 1 was slightly higher than that of *G. polygramma* ribotype 2 (Table 2), more morphological features and molecular information on isolates of *G. polygramma* from other origins are required for a better understanding of the phylogenetic and taxonomical relationships between ribotypes.

Our molecular results revealed a close relationship between *G. geomunensis*, *G. hyalina* and *G. polygramma*. This may be related to the dextral torsion and the plate 1a shared by these species, although the presence of plate 1a is very variable even within the same strain. Despite the similarity in some morphological features, *G. geomunensis* can be distinguished from *G. hyalina* and *G. polygramma* by cell size, and in particular, cell plate ornamentation in

G. geomunensis makes the species distinguishable from *G. hyalina* and *G. polygramma*. In conclusion, based on the morphological differences from other *Gonyaulax* species and phylogenetic positions, we propose *G. geomunensis* as a new species.

Different growth responses to changes in temperature and salinity

In addition to the differences in morphology and phylogenetic positions, *G. whaseongensis*, *G. polygramma* and *G. geomunensis* had a different growth response to changes of temperature and salinity, respectively. For temperature and salinity conditions, the growth ranges of *G. geomunensis* are much narrower than those of *G. whaseogensis* and *G. polygramma*, and *G. whaseongensis* can grow over a wider range of salinities (15–40) than *G. polygramma* (20–40). Similar species-specific responses have also been reported in other dinoflagellates, such as *Alexandrium*, *Gambierdiscus* and *Ostreopsis* (e.g. Lim and Ogata 2005; Kibler *et al*. 2012; Tawong *et al*. 2015). Consequently, it is possible that morphological and phylogenetic identification of *Gonyaulax* species can be supported by differences in growth responses of *Gonyaulax* species to changes of temperature and salinity.

The growth experiments revealed that *G. geomunensis* is stenothermic and stenohaline. High growth of this species would be predicted to occur at the beginning and end of the warm season, when the water temperature is around 25℃ and moderate salinities (25–30) occur. In Korean coastal areas, lower salinity waters (<25) occur in the enclosed bays that receive the input of fresh water from the many streams and rivers during the summer monsoon (Jang *et al*. 2010a; Lee *et al*. 2014). These conditions can inhibit the growth of *G. geomunensis*, indicating that *G. geomunensis* is likely to prefer an oceanic habitat. In contrast, *G. whaseongensis* exhibited a strong tolerance to salinity changes, indicating a euryhaline species. The growth increased at temperatures ≥20℃, and the maximum growth rate of *G. whaseongensis* was about twice those of *G. geomunensis* and *G. polygramma*. Lim *et al*.

(2018) recorded the occurrences of *G. whaseongensis* from the Jangmok Harbor and the waters of Whaseong City, near Shiwha Bay, in summer. These areas receive seasonal outflow from several streams and ditches (Jang *et al*. 2010a; Jang *et al*. 2010b; Shin *et al.* 2000). In this study, *G. whaseongensis* was also collected from Gwangyang Bay, an area strongly affected by fresh water input from Semjin River. It is possible that *G. whaseongensis* has a growth advantage in the neritic habitat, especially in summer.

A dense bloom caused by *G. polygramma* was first recorded in the southern coastal area of Korea, and was associated with a temperature of 25℃ (Cho 2005). In this study, the highest growth rate of *G. polygramma* was also observed at a temperature of 25℃. However, in other areas such as the Bay of Agu, Japan (Nishikawa 1901), the southeastern Arabian Sea (Padmakumar *et al*. 2018; Kumar *et al*. 2020; Dolatabadi *et al*. 2021) and the Gulf of California (Gárate-Lizárraga *et al*. 2006), the blooms have coincided with temperatures between 26 and 29℃. This is not surprising as the higher growth rates of *G. polygramma* in our growth experiments were recorded at high temperatures. According to Tomas (1997), *G. polygramma* is a neritic and oceanic species, indicating that it may have a high tolerance to salinity changes, as shown in our growth experiments. Interestingly, despite the fact that both ribotypes of *G. polygramma* exhibited similar growth responses to changes of temperature and salinity, ribotype 1 is widely distributed along Korean coastal waters, whereas ribotype 2 seems to be restricted to the waters of Geomun Island, Korea (Fig. 1; Table 1). This might be attributed to the intra- and interspecific competition for nutrients and to dispersal by currents, because the distributions of harmful dinoflagellates such as *M. polykrikoides* and *Prorocentrum obtusidens* J. Schiller (formerly *P. donghaiense* D. Lu) in the Korean coastal area are strongly affected by the freshwater intrusion of Changjiang River, China, and the Tsushima Warm Current (Matsuoka *et al*. 2010; Shin *et al*. 2010; Shin *et al*. 2019). However,

it is currently difficult to understand the differences in distribution of the ribotypes of *G. polygramma*, and further studies in other coastal waters are needed.

Formal taxonomic description

Gonyaulax geomunensis* Hyun Jung Kim, Zhun Li, H. Gu, K.N. Mertens & H.H. Shin *sp. nov.

Figs 2–27

DESCRIPTION: The plate formula is Po, *4′, 1a, 6′′, 6C, 5S, 5′′′, 2p, 1′′′′. Cells are ovoidal with a pronounced and slightly angled apex to the right, and a rounded hypotheca without antapical spines or with one, two or three prominent, short and curved antapical spines on the rim of 2p touching 1′′′′. Cell surface is thick and heavily reticulated, with numerous polygonal depressions. The reticulation is deeply excavated. The apical pore complex is surrounded by raised ridges of *4′a, 1′ and 2′, and is smooth and lenticular. A very small intercalary plate surrounded by plates 2′, *3′, and 3′′ is visible in the middle of dorsal area, which is difficult to observe because of the pronounced reticulation. The theca displays dextral torsion. The cingulum is excavated and descends without overhang. Plate 1p is quadrangular and surrounded by *2′′′, *3′′′ and 1′′′′. The chloroplast is parietal; its shape was unclear. A subspherical nucleus is located in the hypotheca.

HOLOTYPE: SEM stub LMBE202201, deposited at the Library of Marine Samples, Korea Institute of Ocean Science & Technology, Geoje 53201, Republic of Korea. The holotype consists of critical-point dried material from monoclonal culture LIMS-PS-3344. Figures 8–23 illustrate cells from this stub.

GENE SEQUENCES: Nuclear-encoded SSU and LSU rDNA (D1–D3 and D8–D10 regions) of strain LIMS-PS-3344 were sequenced. GenBank accessions: OM692364 and OM729600, respectively.

TYPE LOCALITY: Marine waters surrounding Geomun Island, Korea (34°1.125′N, 127°18.138′E).

ETYMOLOGY: The specific epithet *geomunensis* is derived from Geomun Island and refers to the geographic area where the type material was collected.

ACKNOWLEDGEMENTS

This work was supported by grants from Taxonomic Research funded by the National Marine Biodiversity Institute of Korea (2022M01100), Honam National Institute of Biological Resources (HNIBR202101111), Korean culture collection of microalgae and collaboration center (NRF-2022M3H9A1083416), Techniques development for management and evaluation of biofouling on ship hulls (20210651) and National Natural Science Foundation of China (42076085).

REFERENCES

Aguilera-Belmonte A., Inostroza I., Saéz Carrillo K.S., Franco J.M., Riobó P. & Gómez P.I. 2013. The combined effect of salinity and temperature on the growth and toxin content of four Chilean strains of *Alexandrium catenella* (Whedon and Kofoid) Balech 1985 (Dinophyceae) isolated from an outbreak occurring in southern Chile in 2009. *Harmful Algae* 23: 55–59. DOI: 10.1016/j.hal.2012.12.006.

Al Gheilani H.M., Matsuoka K., Alkindi A.Y., Amer S. & Waring C. 2011. Fish kill incidents and harmful algal blooms in Omani Waters. *Agricultural and Marine Sciences* 16: 23–33.

Álvarez C., Uribe E., Regueiro J., Blanco J. & Fraga S. 2016. *Gonyaulax taylorii*, a new yessotoxins-producer dinoflagellate species from Chilean waters. *Harmful Algae* 58: 8–15. DOI: 10.1016/j.hal.2016.07.006.

Andreis C., Ciapi M.D. & Rodondi G. 1982. The thecal surface of some dinophyceae: a comparative SEM approach. *Botanica Marina* 25: 225–236. DOI: 10.1515/botm.1982.25.5.225.

Balech E. 1988. Los dinoflagelados del Atlántico sudoccidental. *Publicaciones Especiales Instituto Español de Oceanografia* 1: 1–310.

Barwani M. 1976. Report of Salalah Investigation (Unpublished Ministry Report).

Carbonell-Moore C. & Mertens K.N. 2019. Should *Gonyaulax hyalina* and *Gonyaulax fragilis* (Dinophyceae) remain two different taxa? *Phycologia* 58: 1–5. DOI: 10.1080.00318884.2019.1663477.

Carbonell-Moore C., Matsuoka K. & Mertens K.N. 2022. Gonyaulacalean tabulation revisited using plate homology and plate overlap, with emphasis on the ventral area (Dinophyceae). *Phycologia* 61: 195–210. DOI: 10.1080/00318884.2021.2024413.

Chikwililwa C., McCarron P., Waniek J.J. & Schulz-Bull D.E. 2019. Phylogenetic analysis and yessotoxin profiles of *Gonyaulax spinifera* cultures from the Benguela Current upwelling system. *Harmful Algae* 85: Article 101626. DOI: 10.1016/j.hal.2019.101626.

Cho E.S. & Choi Y.K. 2005. The characteristics of marine environment and phytoplankton community around southwestern waters for ichthyotoxic dinoflagellate *Cochlodinium polykrikoides* monitoring programme. *Journal of Environmental Sciences* 14: 177–184. DOI: 10.5322/JES.2005.14.2.177.

Darriba D., Taboada G.L., Doallo R. & Posada D. 2012. jMod-elTest 2: more models, new heuristics and parallel computing. *Nature Methods* 9: 772.

Diesing K.M. 1866. Revision der Prothelminthen, Abtheilung: Mastigophoren. *Sitzungsberichte der Kaiserlichen Akademie der Wissenschaften, Mathematisch-Naturwissenschaftliche Classe, Abtheilung I* 52: 287–401.

Dodge J.D. 1988. An SEM study of thecal division in *Gonyaulax* (Dinophyceae). *Phycologia* 27: 241–247. DOI: 10.2216/i0031–8884–27–2–241.1

Dodge J.D. 1989. Some revisions of the family Gonyaulacaceae (Dinophyceae) based on a scanning electron microscope study. *Botanica Marina* 32: 275–298. DOI: 10.1515/botm/1989.32.4.275.

Dolatabadi F., Attaran-Fariman G. & Loghmani M. 2021. Bloom occurrence and phylogeny of *Gonyaulax polygramma* (Dinophyceae) isolated from south east coast of Iran (Oman Sea). *Iranian Journal of Fisheries Sciences* 20: 1789–1803. DOI: 10.22092/IJFS.021.125501.

Ellegaard M., Lewis J. & Harding I. 2002. Cyst-theca relationship, life cycle, and effects of temperature and salinity on the cyst morphology of *Gonyaulax baltica* sp. nov. (Dinophyceae) from the Baltic Sea area. *Journal of Phycology* 38: 775–789. DOI: 10.1046/j.1529–8817.2002.01062.x.

Ellegaard M., Daugbjerg N., Rochon A., Lewis J. & Harding I. 2003. Morphological and LSU rDNA sequence variation within the *Gonyaulax spinifera-Spiniferites* group (Dinophyceae) and proposal of *G. elongata* comb. nov. and *G. membranacea* comb. nov. *Phycologia* 42: 151–164. DOI: 10.2216/i0031–8884–42–2–151.1.

Escalera L., Italiano A., Pistocchi R., Montresor M. & Zingone A. 2018. *Gonyaulax hyalina* and *Gonyaulax fragilis* (Dinoflagellata), two names associated with 'mare sporco', indicate the same species. *Phycologia* 57: 453–464. DOI: 10.2216/17–64.1.

Etheridge S.M. & Roesler C.S. 2005. Effects of temperature, irradiance, and salinity on photosynthesis, growth rates, total toxicity, and toxin composition for *Alexandrium fundyense* isolates from the Gulf of Maine and Bay of Fundy. *Deep-Sea Research II* 52: 2491–2500. DOI: 10.1016/j.dsr2.2005.06.026.

Gárate-Lizárraga I., Muñetón-Gómez M.D.S. & Maldonado-López V.M. 2006. Florecimiento del dinoflagelado *Gonyaulax polygramma* frente a la Isla Espíritu Santo, Golfo de California, México. *Revista de Investigaciones Marinas* 27: 31–39.

Gómez F. 2012. A checklist and classification of living dinoflagellates (Dinoflagellata, Alveolata). *CICIMAR Oceánides* 27: 65–140. DOI: 10.37543/oceanides.v27i1.111.

Grindley J., Taylor F. & Day J. 1964. Red water and marine fauna mortality near Cape Town. *Transactions of the Royal Society of South Africa* 37: 111–130. DOI: 10.1080/00359196409519061.

Gu H., Huo K., Krock B., Bilien G., Pospelova V., Li Z., Carbonell-Moore C., Morquecho L., Ninčevic Ž. & Mertens K.N. 2021. Cyst-theca relationships of *Spiniferites bentorii*, *S. hyperacanthus*, *S. ramosus*, *S. scabratus* and molecular phylogenetics of *Spiniferites* and *Tectatodinium* (Gonyaulacales, Dinophyceae). *Phycologia* 60: 332–353. DOI: 10.1080/00318884.2021.1930796.

Gu H., Mertens K.N., Darrien A., Bilien G., Li Z., Hess P., Séchet V., Krock B., Amorim A., Li Z., Pospelova V., Smith K.F., MacKenzie L., Yoon J.Y., Kim H.J. & Shin H.H. 2022. Unraveling the *Gonyaulax baltica* species complex: cyst-theca relationship of *Impagidinium variaseptum*, *Spiniferites pseudodelicatus* sp. nov. and *S. ristingensis* (Gonyaulacaceae, Dinophyceae), with descriptions of *Gonyaulax bohaiensis* sp. nov, *G. amoyensis* sp. nov. and *G. portimonensis* sp. nov. *Journal of Phycology*, published online DOI: 10.1111/jpy.13245.

Guillard R.R.L. 1973. Division rates. In: *Handbook of phycological methods: culture methods and growth measurements* (Ed. by J.R. Stein), pp 289–311. Cambridge University Press, Cambridge, UK.

Han K.H., Li Z., Kang B.J., Youn J.Y. & Shin H.H. 2019. Toxin dinoflagellate *Gymnodinium catenatum* Graham (Dinophyceae) from the southern coast of Korea: morphology, phylogeny and effects of temperature and salinity on growth. *Korean Journal of Environmental Biology* 37: 31–41. DOI: 10.11626/KJEB.2019.37.1.031.

Hansen G., Moestrup Ø. & Roberts K.R. 1996. Fine structural observations on *Gonyaulax spinifera* (Dinophyceae), with special emphasis on the flagellar apparatus. *Phycologia* 35: 354–366. DOI: 10.2216/i0031–8884–35–4–354.1.

Iwataki M., Kawami H., Mizushima K., Mikulski C.M., Doucette G.J., Relox Jr J.R., Anton A., Fukuyo Y. & Matsuoka K. 2008. Phylogenetic relationships in the harmful dinoflagellate *Cochlodinium polykrikoides* (Gymnodiniales, Dinophyceae) inferred from LSU rDNA sequences. *Harmful Algae* 7: 271–277. DOI: 10.1016/j.hal.2007.12.003.

Jang P.G., Jang M.C., Lee W.J. & Shin K. 2010a. Effects of nutrient property changes on summer phytoplankton community structure of Jangmok Bay. *Ocean and Polar Research* 32: 97–111. DOI: 10.4217/OPR.2010.32.2.097.

Jang M.C., Shin K., Jang P.G. & Lee W.J. 2010b. Relationship between environmental factors and short-term variations of mesozooplankton during summer in Jangmok Bay, South Coast of Korea. *Ocean and Polar Research* 32: 41–52. DOI: 10.4217/OPR.2010.32.1.041.

Jeong H.J., Lee K.H., Yoo Y.D., Kang N.S., Song J.Y., Kim T.H., Seong K.A., Kim J.S. & Potvin E. 2018. Effects of light intensity, temperature, and salinity on the growth and ingestion rates of the red-tide mixotrophic dinoflagellate *Paragymnodinium shiwhaense*. *Harmful Algae* 80: 46–54. DOI: 10.1016/j.hal.2018.09.005.

Kang S.M. & Lee J.B. 2018. New records of genus *Dinophysis*, *Gonyaulax*, *Amphidinium*, *Heterocapsa* (Dinophyceae) from Korea waters. *Korean Journal of Environment Biology* 36: 260–270. DOI: 10.11626/KJEB.2018.36.3.260.

Katoh K., Rozewicki J. & Yamada K.D. 2019. MAFFT online service: multiple sequence alignment, interactive sequence choice and visualization. *Briefings in Bioinformatics* 20: 1160–1166. DOI: 10.1093/bib/bbx108.

Kibler S.R., Litaker R.W., Holland W.C., Vandersea M.W. & Tester P.A. 2012. Growth of eight *Gambierdiscus* (Dinophyceae) species: effects of temperature, salinity and irradiance. *Harmful Algae* 19: 1–14. DOI: 10.1016/j.hal.2012.04.007.

Kim D.I., Matsuyama Y., Nagasoe S., Yamaguchi M., Yoon Y.H., Oshima Y., Imada N. & Honjo T. 2004. Effects of temperature, salinity and irradiance on the growth of the harmful red tide dinoflagellate *Cochlodinium polykrikoides* Margalef (Dinophyceae). *Journal of Plankton Research* 26: 61–66. DOI: 10.1093/plankt/fbh001.

Kofoid C.A. 1911. Dinoflagellate of the San Diego region, Ⅳ. The genus *Gonyaulax*, with notes on its skeletal morphology and a discussion of its generic and specific characters. *University of California Publications in Zoology* 8: 187–287.

Koizumi Y., Kohno J., Matsuyama N., Uchida T. & Honjo T. 1996. Environmental features and the mass mortality of fish and shellfish during the *Gonyaulax polygramma* red tide occurred in and around Uwajima Bay, Japan, in 1994. *Nippon Suisan Gakkaishi* 62: 217–224.

Kretschmann J., Čalasan A.J., Knechtel J., Owsianny P.M., Facher E. & Gottschling M. 2022. Evolution of Thoracosphaeroideae (Peridiniales, Dinophyceae) and a case of atavism in taxonomically clarified *Chimonodinium lomnickii* var. *wierzejskii* from the Polish Tatra Mountains. *European Journal of Phycology*, published online. DOI: 10.1080/09670262.2021.2002950.

Kumar P.S., Kumaraswami M., Ezhilarasan P., Rao G.D., Sivasankar R., Rao V.R. & Ramu K. 2020. Blooming of *Gonyaulax polygramma* along the southeastern Arabian Sea: influence of upwelling dynamics and anthropogenic activities. *Marine Pollution Bulletin* 151: Article 110817. DOI: 10.1016/j.marpolubul.2019.110817.

Lebour M.V. 1925. *The dinoflagellates of the northern Seas*. Marine Biological Association, London, UK. 250 pp.

Lee C.K., Min H.C., Lee S.G., Jung C.S., Kim H.G. & Lim W.A. 2001. Abundance of harmful algae, *Cochlodinium polykrikoides*, *Gyrodinium impudicum* and *Gymnodinium catenatum* in the coastal area of South Sea of Korea and their effects of temperature, salinity, irradiance and nutrient on the growth in culture. *Journal of Korean Society of Fisheries and Aquatic Science* 34: 536–544.

Lee S.W, Park C., Lee D.B. & Lee J.G. 2014. Effects of freshwater discharge on plankton in Cheonsu Bay, Korea during the rainy season. *Journal of the Korean Society of Oceanography* 19: 41–52. DOI: 10.7850/jkso.2014.19.1.41.

Lemmermann E. 1903. Brandenburgische Algen. II. Das Phytoplankton des Müggelsees und einiger benachbarter Gewässer. *Zeitschrift für Fischerei und deren Hilfswissenschaften* 11: 73–123.

Lewis J., Rochon A. & Harding I. 1999. Preliminary observations of cyst-theca relationship in *Spiniferites ramosus* and *Spiniferites membranaceus* (Dinophyceae). *Grana* 38: 113–124. DOI: 10.1080/00173139908559220.

Lewis J., Rochon A., Ellegaard M., Mudie P.J. & Harding I. 2001. The cyst-theca relationship of *Bitectatodinium tepikiense* (Dinophyceae). *European Journal of Phycology* 36: 137–146. DOI: 10.1017/s0967026201003171.

Li Z., Han M.S., Matsuoka K., Kim S.O. & Shin H.H. 2015. Identification of the resting cyst of *Cochlodinium polykrikoides* Margalef (Dinophyceae, Gymnodiniales) in Korea coastal sediments. *Journal of Phycology* 51: 204–210. DOI: 10.1111.jpy.12252.

Li Z., Park J.S., Kang N.S., Chomérat N., Mertens K.N., Gu H., Lee K.W., Kim K.H., Baek S.H., Shin K. *et al.* 2021. A new potentially toxic dinoflagellate *Fukuyoa koreansis* sp. nov. (Gonyaulacales, Dinophyceae) from Korean coastal waters: morphology, phylogeny, and effects of temperature and salinity on growth. *Harmful Algae* 109: Article 102107. DOI: 10.1016/j.hal.2021.102107.

Lim P.T. & Ogata T. 2005. Salinity effect on growth and toxin production of four tropical *Alexandrium* species (Dinophyceae). *Toxicon* 45: 699–710. DOI: 10.1016/j.toxicon.2005.01.007.

Lim A.S., Jeong H.J., Kwon J.E., Lee S.Y. & Kim J.H. 2018. *Gonyaulax whaseongensis* sp. nov. (Gonyaulacales, dinophyceae), a new phototrophic species from Korean coastal waters. *Journal of Phycology* 54: 923–928. DOI: 10.1111/jpy.12792.

Matsubara T., Nagasoe S., Yamasaki Y., Shikata T., Shimasaki Y., Oshima Y. & Honjo T. 2007. Effects of temperature, salinity, and irradiance on the growth of the dinoflagellate *Akashiwo sanguinea*. *Journal of Experimental Marine Biology and Ecology* 342: 226–230. DOI: 10.1016/j.jembe.2006.09.013.

Matsuoka K., Mizuno A., Iwataki M., Takano Y., Yamatogi T., Yoon Y.H. & Lee J.B. 2010. Seed populations of a harmful unarmored dinoflagellate *Cochlodinium polykrikoides* Margalef in the East China Sea. *Harmful Algae* 9: 548–556. DOI: 10.1016/j.hal.2010.04.003.

Mertens K.N., Aydin H., Uzar S., Takano Y., Yamaguchi A. & Matsuoka K. 2015. Relationship between the dinoflagellate cyst *Spiniferites pachydermus* and *Gonyaulax ellegaardiae* sp. nov. from Izmir bay, Turkey, and molecular characterization. *Journal of Phycology* 51: 560–573. DOI: 10.1111/jpy.12304.

Mertens K.N., Takano Y., Gu H., Bagheri S., Pospelova V., Pieńkowski A.J., Leroy S.A.G & Matsuoka K. 2017. Cyst-theca relationship and phylogenetic position of *Impagidinium caspienense* incubated from Caspian Sea surface sediments: relation to *Gonyaulax baltica* and evidence for heterospory within gonyaulacoid dinoflagellates. *Journal of Eukaryotic Microbiology* 64: 829–842. DOI: 10.1111/jeu.12417.

Morton S.L. & Villareal T.A. 1998. Bloom of *Gonyaulax polygramma* Stein (Dinophyceae) in a coral reef mangrove lagoon, Douglas Cay, Belize. *Bulletin of Marine Science* 63: 639–642.

Nagasoe S., Kim D.I., Shimasaki Y., Oshima Y., Yamaguchi M. & Honjo T. 2006. Effects of temperature, salinity and irradiance on the growth of the red tide dinoflagellate *Gymnodinium instriatum* Freudenthal et Lee. *Harmful Algae* 5: 20–25. DOI: 10.1016/j.hal.2005.06.001.

Nishikawa T. 1901. *Gonyaulax* and the discolored water in the Bay of Agu. *Annotationes Zoologicae Japonenses* 4: 31–34. DOI: 10.34434/za000041.

Oh S.J., Park J.A., Kwon H.K., Yang H.S. & Lim W.A. 2012. Ecophysiological studies on the population dynamics of two toxic dinoflagellates *Alexandrium tamarense* and *Alexandrium catenella* isolated from Southern Coast of Korea Ⅰ. Effects of temperature and salinity on the growth. *Journal of the Korean Society of Marine Environmental Engineering* 15: 133–141. DOI: 10.7846/JKOSMEE.2012.15.2.133.

Padmakumar K.B., Thomas L.C., Salini T.C., Vijayan A. & Sudhakar M. 2018. Subsurface bloom of dinoflagellate *Gonyaulax polygramma* Stein in the shelf waters off Mangalore-South Eastern Arabian Sea. *Indian Journal of Geo Marine Sciences* 47: 1658–1664.

Park B.S., Kim J.H., Kim J.H., Baek S.H. & Han M.S. 2018. Intraspecific bloom succession in the harmful dinoflagellate *Cochlodinium polykrikoides* (Dinophyceae) extended the blooming period in Korean coastal waters in 2009. *Harmful Algae* 71: 78–88. DOI: 10.1016/j.hal.2017.12.004.

Park J.S., Li Z., Kim H.J., Kim K.H., Lee K.W., Youn J.Y., Kwak K.Y. & Shin H.H. 2021. First report of the marine benthic dinoflagellate *Bysmatrum subsalsum* from Korean tidal pools. *Journal of Marine Science and Engineering* 9: Article 649. DOI: 10.3390/jsme9060649.

Pitcher G.C., Foord C.J., Mecey B.M., Mansfield L., Mouton A., Smith M.E., Osmond S.J. & van der Molen L. 2019. Devastating farmed abalone mortalities attributed to yessotoxin-producing dinoflagellates. *Harmful Algae* 81: 30–41. DOI: 10.1016.j.hal.2018.11.006.

Rhodes L., McNabb P., Salas M.D., Briggs L., Beuzenberg V. & Gladstone M. 2006. Yessotoxin production by *Gonyaulax spinifera*. *Harmful Algae* 5: 148–155. DOI: 10.1016/j.hal.2005.06.008.

Riccardi M., Guerrini F., Roncarati F., Milandri A., Cangini M., Pigozzi S., Riccardi E., Ceredi A., Ciminiello P., Dell'Aversano C. *et al.*. 2009. *Gonyaulax spinifera* from the Adriatic sea: toxin production and phylogenetic analysis. *Harmful Algae* 8: 279–290. DOI: 10.1016/j.hal.2008.06.008.

Ronquist F., Teslenko M., van der Mark P., Ayres D.L., Darling A., Hohna S., Larget B., Liu L., Suchard M.A. & Huelsenbeck J.P. 2012. MrBayes 3.2: efficient Bayesian

phylogenetic inference and model choice across a large model space. *Systematic Biology* 61: 539–542. DOI: 10.1093/sysbio/sys029.

Schiller J. 1937. Dinoflagellatae (Peridineae) in monographischer Behandlung. In: *Rabenhorst's Kryptogamen-flora von Deutschland, Österreich und der Schweiz*, ed. 2, vol. 10 (3), part 2 (Ed. by R. Kolkwitz). Akademische Verlagsgesellschaft, Leipzig, Germany. 590 pp.

Shin J.K., Kim D.S. & Cho K.J. 2000. Dynamics of inorganic nutrients and phytoplankton in Shihwa Reservoir. *Korean Journal of Limnology* 33: 109–118.

Shin H.H., Matsuoka K., Yoon Y.H. & Kim Y.O. 2010. Response of dinoflagellate cyst assemblages to salinity changes in Yeoja Bay, Korea. *Marine Micropaleontology* 77: 15–24. DOI: 10.1016/j.marmicro.2010.07.001.

Shin H.H., Li Z., Seo M.H., Soh H.Y., Lim W.A. & Park J.W. 2019. Harmful dinoflagellate *Prorocentrum donghaiense* Lu is widely distributed along the East China Sea and Korean Coastal Area. *Ocean Science Journal* 54: 685–691.

Sournia A. 1984. Classification et nomenclature de divers dinoflagellés marins (Dinophyceae). *Phycologia* 23: 345–355. DOI: 10.2216/i0031–8884–23–3–345.1.

Stamatakis A. 2014. RAxML version 8: a tool for phylogenetic analysis and post-analysis of large phylogenies. *Bioinformatics* 30: 1312–1313. DOI: 10.1093/bioinformatics/btu033/.

Stein, F. 1883. *Der Organismus der Infusionsthiere… III. Abtheilung. II. Hälfte. Die Naturgeschichte der arthrodelen Flagellaten. Einleitung und Erklärung der Abbildungen.* Wilhelm Engelmann, Leipzig, Germany. 30 pp, 25 pls.

Stover L.E. & Evitt W.R. 1978. Analyses of pre-Pleistocene organic-walled dinoflagellates. *Stanford University Publications, Geological Sciences* 15: 1–300.

Takano Y. & Horiguchi T. 2004. Surface ultrastructure and molecular phylogenetics of four unarmoured heterotrophic dinoflagellates including the type species of the genus *Gyrodinium* (Dinophyceae). *Phycological Research* 52: 107–116. DOI: 10.1111/j.1440-183.2004.00332.x

Takano Y. & Horiguchi T. 2006. Acquiring scanning electron microscopical, light microscopical and multiple gene sequence data from a single dinoflagellate cell. *Journal of Phycology* 42: 251–256. DOI: 10.1111/j.1529–8817.2006.00177.x.

Tamura K., Stecher G. & Kumar S. 2021. MEGA11: molecular evolutionary genetics analysis version 11. *Molecular Biology and Evolution* 37: 3022–3027. DOI: 10.1093/molbev/msab120.

Tawong W., Yoshimatsu T., Yamaguchi H. & Adachi M. 2015. Effects of temperature, salinity and their interaction on growth of benthic dinoflagellates *Ostreopsis* spp. from Thailand. *Harmful Algae* 44: 37–45. DOI: 10.1016/j.hal.2015.02.011.

Taylor F.J.R. 1962. *Gonyaulax polygramma* Stein in Cape water: a taxonomic problem related to developmental morphology. *South African Journal of Botany* 28: 237–242.

Tomas C.R. [Ed.] 1997. *Identifying marine phytoplankton*. Academic Press, San Diego, California, USA. 858 pp.

Vaidya G., Lohman D.J. & Meier R. 2011. SequenceMatrix: concatenation software for the fast assembly of multi-gene datasets with character set and codon information. *Cladistics* 27: 171–180.

van der Lingen C.D., Hutchings L., Lamont T. & Pitcher G.C. 2016. Climate change, dinoflagellate blooms and sardine in the southern Benguela current large marine ecosystem. *Environmental Development* 17: 230–243. DOI: 10.1016/j.envdev.2015.09.004.

Xu N., Duan S., Li A., Zhang C., Cai Z. & Hu Z. 2010. Effects of temperature, salinity and irradiance on the growth of the harmful dinoflagellate *Prorocentrum donghaiense* Lu. *Harmful Algae* 9: 13–17. DOI: 10.1016/j.hal.2009.06.002.

Yamaguchi A. & Horiguchi T. 2005. Molecular phylogenetic study of the heterotrophic dinoflagellate genus *Protoperidinium* (Dinophyceae) inferred from small subunit rRNA gene sequences. *Phycological Research* 53: 30–42. DOI: 10.1111/j.1440–183.2005.00370.x.

Zhang W., Li Z., Mertens K.N., Derrien A., Pospelova V., Carbonell-Moore M.C., Bagheri S., Matsuoka K., Shin H.H. & Gu H. 2020. Reclassification of *Gnyaulax verior* (Gonyaulacales, Dinophyceae) as *Sourniaea diacantha gen. et comb. nov*. *Phycologia* 59: 246–260. DOI: 10.1080/00318884.2020.1735926.

LEGENDS FOR FIGURES

Fig. 1. Locations of the sampling sites in Korean coastal area and East China Sea.

Figs 2–7. Light and fluorescence micrographs of *Gonyaulax geomunensis sp. nov.* (strain LIMS-PS-3344). Scale bars = 10 µm.

Fig. 2. High focus of ventral view showing the cingulum.

Fig. 3. Mid focus showing the cell outline.

Fig. 4. High focus of right lateral view showing the cell surface and cingulum.

Fig. 5. Mid focus of left lateral view showing the nucleus (n).

Fig. 6. Mid focus of dorsal view showing the antapical spines (arrows) and granular contents (arrowheads).

Fig. 7. Ventral view of SYTOX Green-stained cell showing the position of the nucleus (green) and chloroplasts (red).

Figs 8–23. Scanning electron micrographs of *Gonyaulax geomunensis sp. nov.* (strain LIMS-PS-3344). Scale bars = 5 µm.

Fig. 8. Ventral view showing the cingulum and one antapical spine (arrow).

Figs 9–10. Ventral-left lateral view showing two antapical spines (arrows).

Fig. 11. Dorsal view showing the dextral torsion.

Fig. 12. Right lateral view.

Fig. 13. Dorsal view of hypotheca.

Fig.14. Antapical view showing the small pores (arrowheads).

Fig. 15. Partial antapical view showing sulcal area.

Fig. 16. Inside view showing the 1′ plate and ventral pore (arrow).

Figs 17–18. Details of APC with ventral pore (arrows).

Fig. 19. Ventral view showing the 1′ plate.

Fig. 20. Apical view showing APC and the precingular plates.

Fig. 21. Inside view showing 1a plate (arrow).

Fig. 22. Detail of sulcal area.

Fig. 23. Antapical view showing the antapical spines (arrows).

Figs 24–27. Schematic drawings of thecal plate pattern of *Gonyaulax geomunensis*.

Fig. 24. Ventral view.

Fig. 25. Dorsal view.

Fig. 26. Apical view.

Fig. 27. Antapical view.

Figs 28–33. Light and fluorescence micrographs of *Gonyaulax whaseongensis* (Strain LIMS-PS-3443). Scale bars = 10 µm.

Fig. 28. High focus of ventral view showing the sulcal area, the cingulum and the antapical spine (arrow).

Fig. 29. Mid focus showing the nucleus (n).

Fig. 30. Mid focus of left lateral view showing the nucleus.

Fig. 31. Mid focus of right lateral view showing the cingulum.

Fig. 32. High focus of dorsal view showing partly the cingulum.

Fig. 33. Mid focus of dorsal view of SYTOX Green-stained cell showing the position of the nucleus (green) and chloroplast (red).

Figs 34–49. Scanning electron micrographs of *Gonyaulax whaseongensis* (Strain LIMS-PS-3443). Scale bars = 5 µm.

Fig. 34. Ventral view showing an antapical spine (arrow).

Fig. 35. Left lateral view.

Fig. 36. Dorsal view showing the dextral torsion and two antapical spines (arrows).

Fig. 37. Right lateral view.

Fig. 38. Right-antapical view.

Fig. 39. Ventral view showing the S-type ventral organization and two antapical spines (arrows) and small pores (arrowheads).

Fig. 40. Ventral-antapical view showing the sulcal area.

Figs 41–42. Apical view showing the 1′ plate and ventral pore (arrows).

Fig. 43. Right apical view showing the APC and *4′a plate.

Fig. 44. Apical view showing the APC.

Fig. 45. Details of 1′ plate showing a row of small pores (arrows).

Figs 46–48. Details of sulcal area.

Fig. 49. Antapical view showing the antapical spines with wide bases surrounding the boundaries of 2p (arrows).

Figs 50–53. Schematic drawings of thecal plate patterns of *Gonyaulax whaseongensis*.

Fig. 50. Ventral view.

Fig. 51. Dorsal view.

Fig. 52. Apical view.

Fig. 53. Antapical view.

Figs 54–59. Light and fluorescence micrographs of *Gonyaulax polygramma* ribotype 1 (Strain LIMS-PS-3467). Scale bars = 10 μm.

Fig. 54. High focus of ventral view showing the cingular displacement.

Fig. 55. Mid focus showing the nucleus (n) and antapical spine (arrow).

Fig. 56. Mid focus of left lateral view.

Fig. 57. High focus of right lateral view.

Fig. 58. High to mid focus of dorsal view showing the nucleus.

Fig. 59. Mid focus of SYTOX Green-stained cell showing the position of the nucleus (green) and chloroplast (red).

Figs 60–65. Light and fluorescence micrographs of *Gonyaulax polygramma* ribotype 2 (Strain LIMS-PS-3347). Scale bars = 10 µm.

Fig. 60. High focus of ventral view showing the cingulum and antapical spine (arrow).

Fig. 61. High focus of left lateral view.

Fig. 62. Mid focus of left lateral view showing the nucleus (n).

Fig. 63. Mid focus of right lateral view.

Fig. 64. Mid focus of dorsal view showing the nucleus.

Fig. 65. Mid focus of SYTOX Green-stained cell showing the position of the nucleus (green) and chloroplast (red).

Figs 66–78. Scanning electron micrographs of *Gonyaulax polygramma* ribotype 1 (Strain LIMS-PS-3467). Scale bars = 5 µm.

Fig. 66. Ventral view showing the S-type ventral organization, ventral pore (vp) and antapical spine (arrow).

Fig. 67. Ventral-left lateral view.

Figs 68–69. Dorsal view showing the dextral torsion.

Fig. 70. Ventral-right lateral view showing the spines.

Fig. 71. Right apical view, showing ventral pore and the sulcal area.

Fig. 72. Ventral view showing the sulcal area.

Fig. 73. Dorsal view showing 1a plate.

Fig. 74. Dorsal view of cell without 1a plate.

Fig. 75. Apical view showing the APC.

Figs 76–77. Details of sulcal area and small pores on 2p (arrowheads).

Fig. 78. Antapical view showing the antapical spines (arrows) and 2p.

Figs 79–90. Scanning electron micrographs of *Gonyaulax polygramma* ribotype 2 (Strain LIMS-PS-3347). Scale bars = 5 µm.

Fig. 79. Ventral view showing the S-type ventral organization, cingulum, ventral pore (vp) and antapical spine (arrow).

Fig. 80. Left lateral view.

Fig. 81. Dorsal view showing the dextral torsion and 1a plate.

Fig. 82. Ventral-right lateral view showing the APC.

Figs 83–84. Ventral view showing the ventral pore (vp) and *4′a plate.

Fig. 85. Dorsal view showing the 1a plate.

Fig. 86. Left lateral view showing the 1a plate.

Fig. 87. Apical view showing the APC.

Figs 88–89. Details of the sulcal area.

Fig. 90. Antapical view showing the 2p and antapical spine (arrow).

Figs 91–98. Schematic drawing of thecal plate patterns of *Gonyaulax polygramma*.

Fig. 91. Ventral view of *G. polygramma* ribotype 1.

Fig. 92. Dorsal view of *G. polygramma* ribotype 1.

Fig. 93. Ventral view of *G. polygramma* ribotype 2.

Fig. 94. Dorsal view of *G. polygramma* ribotype 2.

Fig. 95. Apical view of *G. polygramma* ribotype 1.

Fig. 96. Antapical view of *G. polygramma* ribotype 1.

Fig. 97. Apical view of *G. polygramma* ribotype 2.

Fig. 98. Antapical view of *G. polygramma* ribotype 2.

Fig. 99. Maximum-likelihood (ML) phylogenetic tree obtained using SSU-LSU concatenated sequences. *Adenoides eludens* was used as outgroup. The numbers on each node are the bootstrap values (%) followed by the Bayesian posterior probability (PP). Only bootstrap values above 50% and PP above 0.7 are shown. Scale bar = 0.05 nucleotide substitutions per site.

Figs 100–103. Contour plots of growth rate (day^{-1}) of *Gonyaulax* species exposed to changes in combinations of salinity and temperature.

Fig. 100. *G. geomunensis sp. nov.*

Fig. 101. *G. whaseongensis*.

Fig. 102. *G. polygramma* ribotype 1.

Fig. 103. *G. polygramma* ribotype 2.

Table legends

Table 1. Information on *Gonyaulax* species identified in this study.

Table 2. Morphological comparisons of *Gonyaulax geomunensis*, *G. whaseongensis* and two ribotypes of *G. polygramma*.

Table 1.

Species	Strains	Collection date	Station	Latitude	Longitude	Temperature (℃)	Salinity	GenBank No. (SSU / LSU)
Gonyaulax geomunensis	LIMS-PS-3344	9 Jul. 2019	3	34˚ 01’ 07.52” N	127˚ 18’ 08.30” E	22.7	-	OM692364/OM729600
Gonyaulax whaseongensis	LIMS-PS-3443	15 Jul. 2020	1	34˚ 51’ 34.16” N	127˚ 43’ 18.87” E	22.7	17	OM692365/OM729601
Gonyaulax polygramma ribotype 1	LIMS-PS-3466	6 Aug. 2019	4	33˚ 00’ 00.00” N	125˚ 30’ 00.00” E	16.0	29.0	OM692366/OM729602
Gonyaulax polygramma ribotype 1	LIMS-PS-3467	6 Aug. 2019	4	33˚ 00’ 00.00” N	125˚ 30’ 00.00” E	16.0	29.0	OM692367/OM729603
Gonyaulax polygramma ribotype 2	LIMS-PS-3346	9 Jul. 2019	2	34˚ 01’ 45.86” N	127˚ 18’ 48.60” E	-	-	OM692368/OM729604
Gonyaulax polygramma ribotype 2	LIMS-PS-3347	9 Jul. 2019	2	34˚ 01’ 45.86” N	127˚ 18’ 48.60” E	-	-	OM692369/OM729605

Table 2.

	G. geomuneensis	***G. whaseongensis***	***G. polygramma*** **ribotype 1**	***G. polygramma*** **ribotype 2**
Overall shape	ovoid	sub-spherical	slightly elongated	slightly elongated
Apical view	circular	circular	sub-circular	sub-circular
Length	25.5–43.9 (33.4 ± 4.2, n=30)	38.6–42.7 (40.6 ± 1.4, n=15)	33.2–44.5 (38.5 ± 2.3, n=32)	32.1–47.9 (36.9 ± 2.9, n=30)
Width (transdiameter)	23.4–35.0 (28.5 ± 2.6, n=30)	31.7–33.4 (32.7 ± 0.6, n=15)	27.6–36.8 (31.0 ± 2.0, n=32)	24.5–37.2 (29.6 ± 2.6, n=30)
Ratio	1.1–1.2 (1.11 ± 0.03, n=16)	1.2–1.3 (1.24 ± 0.04, n=15)	1.1–1.3 (1.24 ± 0.05, n=32)	1.1–1.4 (1.25 ± 0.07, n=30)
Apical horn	Short	short, inconspicuous	stout	stout
Shoulder	weakly angled	slightly angled	pronounced shoulder	pronounced shoulder
Number of antapical spines	1–2 or more, unequal, one often prominent	2, unequal, one often prominent	1–2 or more, unequal, one often prominent	1–2 or more, unequal, one often prominent
Shape of antapical spine	narrow, long and straight	short and sharply pointed	narrow, long and straight	narrow, long and straight
Cingulum width (μm)	2.6–3.7 (2.9 ± 0.4, n=12)	3.1–3.7 (3.23 ± 0.21, n=7)	2.6–4.0 (3.13 ± 0.49, n=7)	3.1–4.4 (3.91 ± 0.72, n=3)
Angle with major axis by line joining ends of cingulum	4.7–23.6 (14.93 ± 7.41, n=12)	2.5–13.0 (6.84 ± 3.79, n=7)	1.9–12.9 (7.55 ± 3.98, n=7)	7.8–9.3 (8.27 ± 0.75, n=3)

Displacement of cingulum relative to cingulum widths	1.3–1.8 (1.53 ± 0.22, n=12)	1.2–2.0 (1.64 ± 0.28, n=7)	1.7–2.1 (1.96 ± 0.14, n=7)	1.3–1.4 (1.34 ± 0.08, n=3)
Overhang of cingulum ends	No	No	No	No
Apical plate 1′	slender, S shape	slender	slender	slender
Row of small pores on plate 1′	No	Yes	No	No
Apical plate 4′	elongated	elongated	pentagonal	pentagonal
Intercalary plate 1a	Yes	No	Yes	Yes
Precingular plate 6″	quadrangular	quadrangular	quadrangular	quadrangular
Postcingular plate 1‴	long and slender, very narrow	long and slender, very narrow	long and slender, very narrow	long and slender, very narrow
Antapical plate 1⁗	pentagonal	pentagonal	pentagonal	pentagonal
Posterior intercalary plate 1p	elongated and wide	elongated and wide	elongated and wide	elongated and wide
Ventral pore	4′	4′	4′	4′
Surface	recticulated and vermiculated	reticulated	linear ridges	linear ridges

Figure 1

Click here to access/download;Figure;Fig. 1.tif

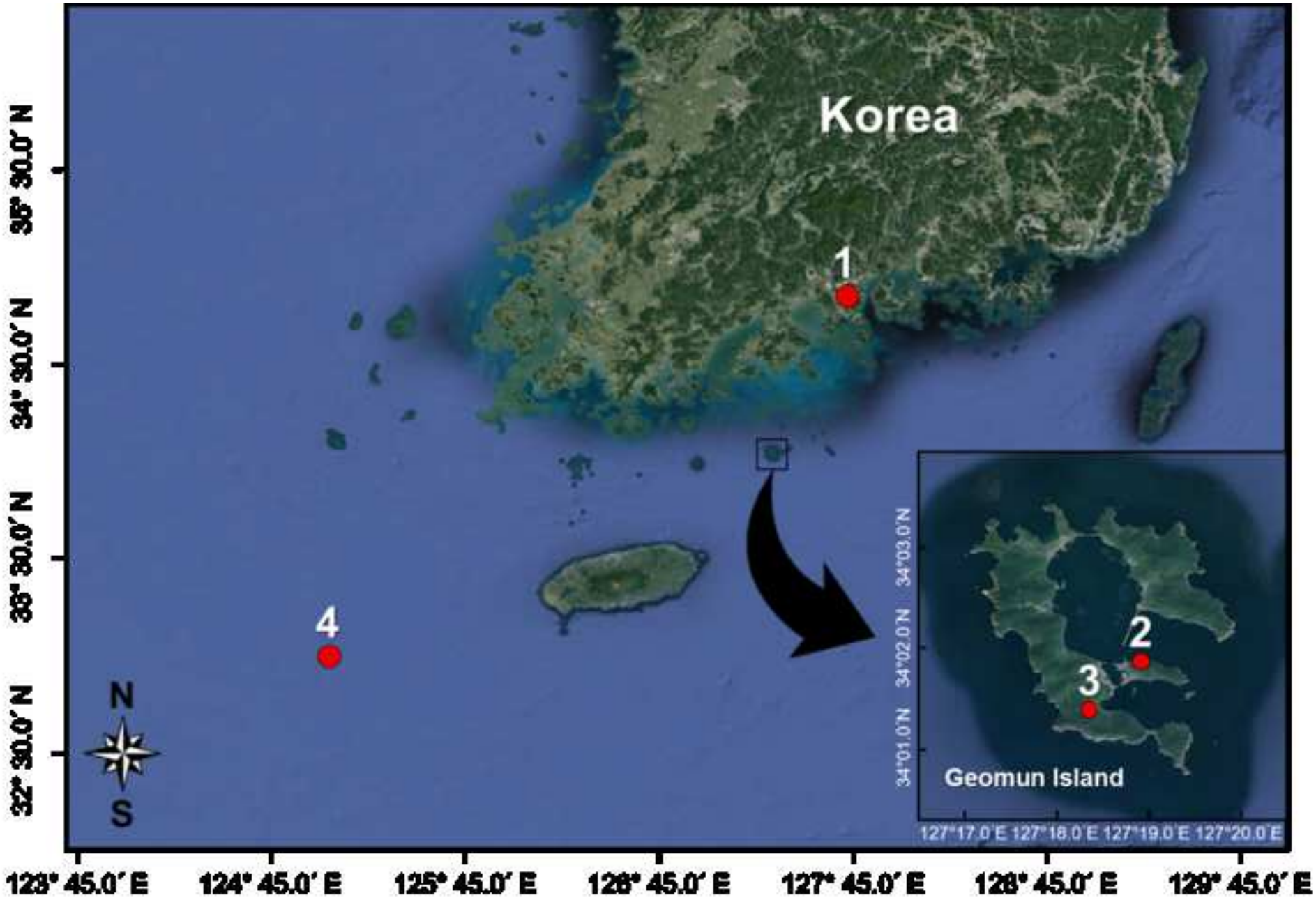

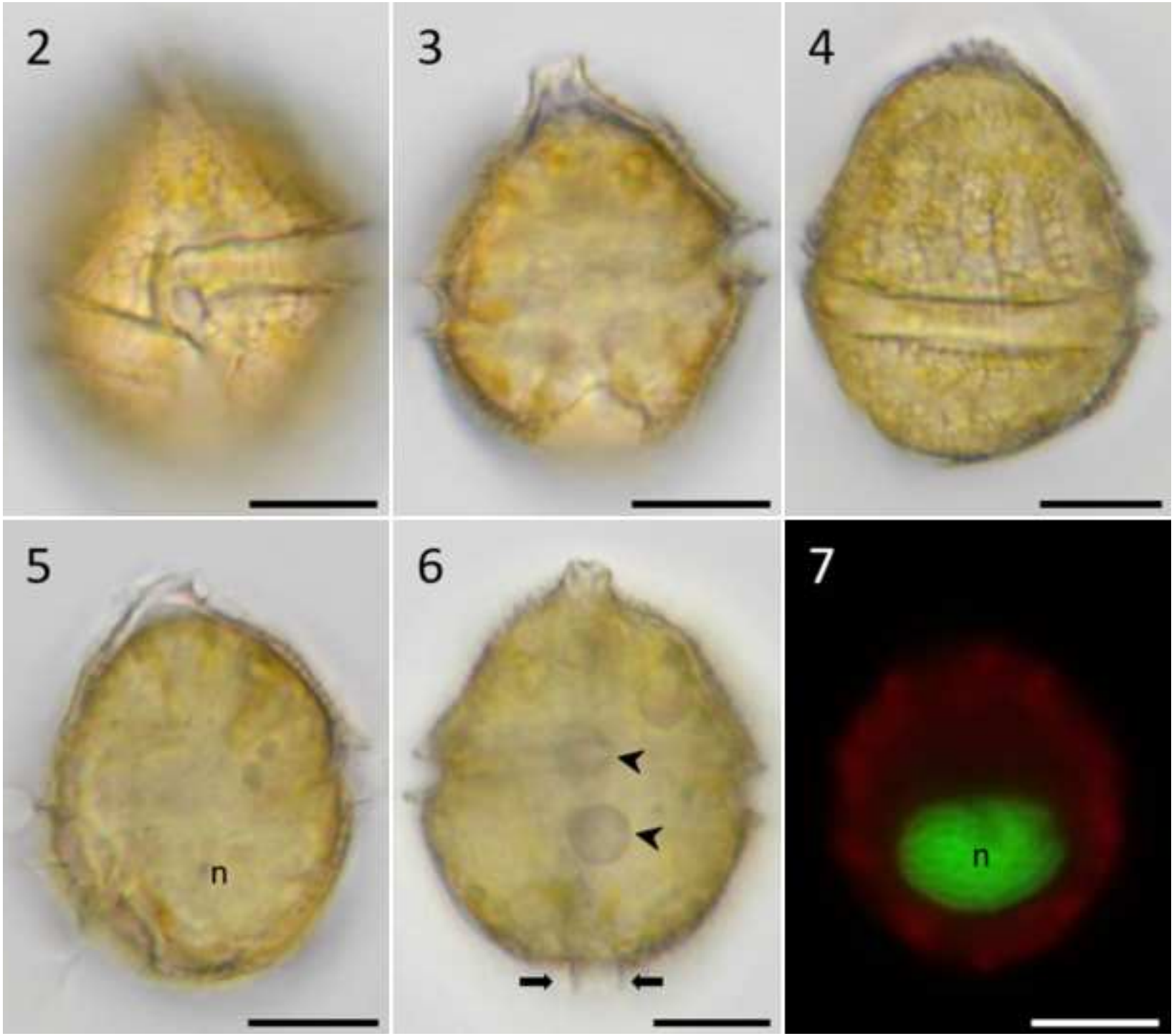

Figures 8-23

Click here to access/download;Figure;Fig. 8-23.tif

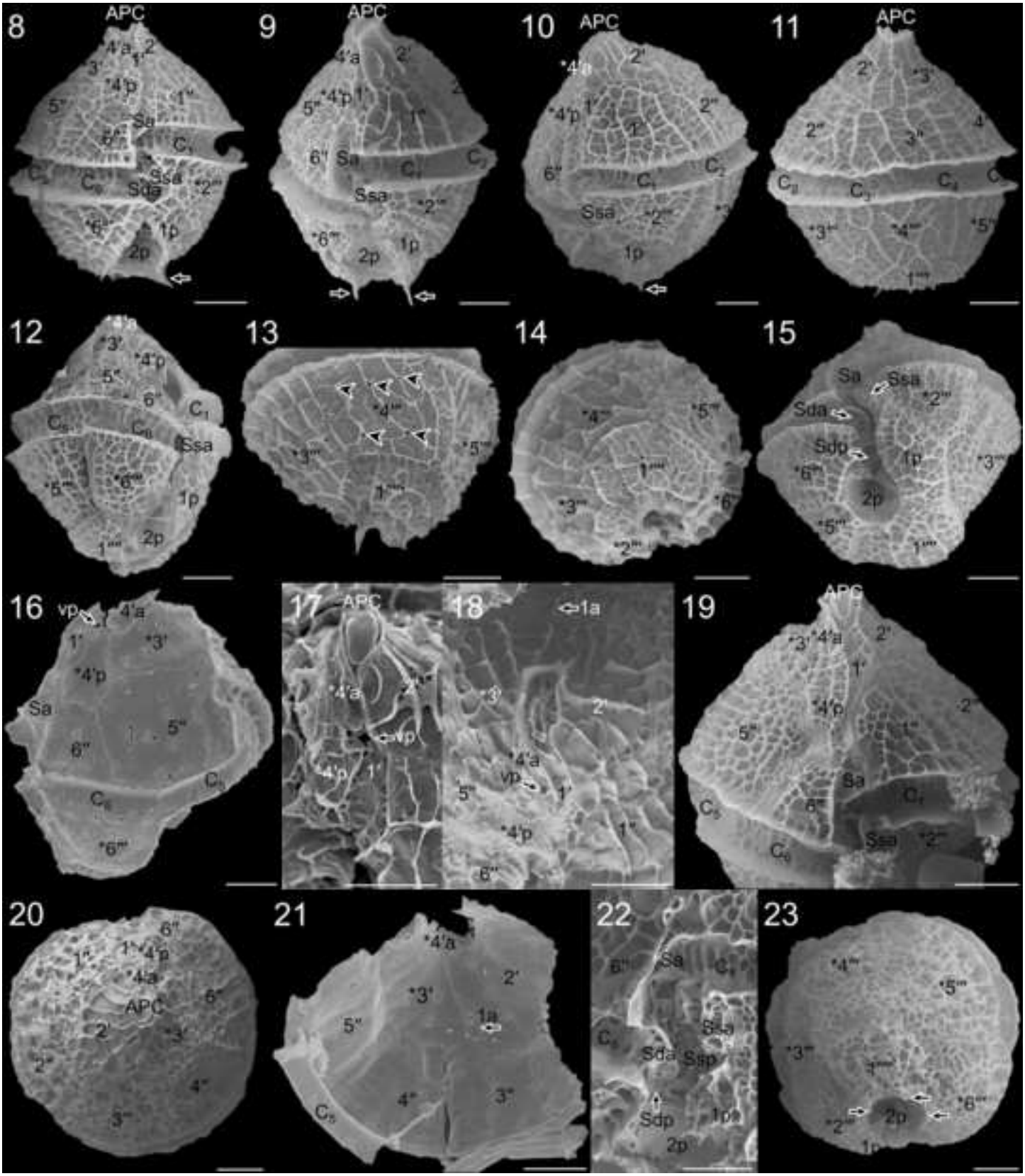

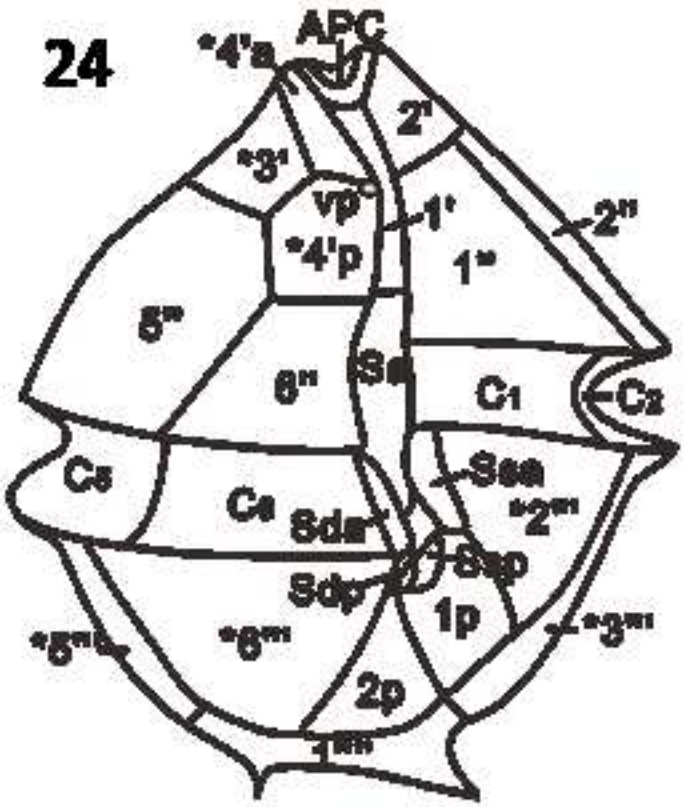

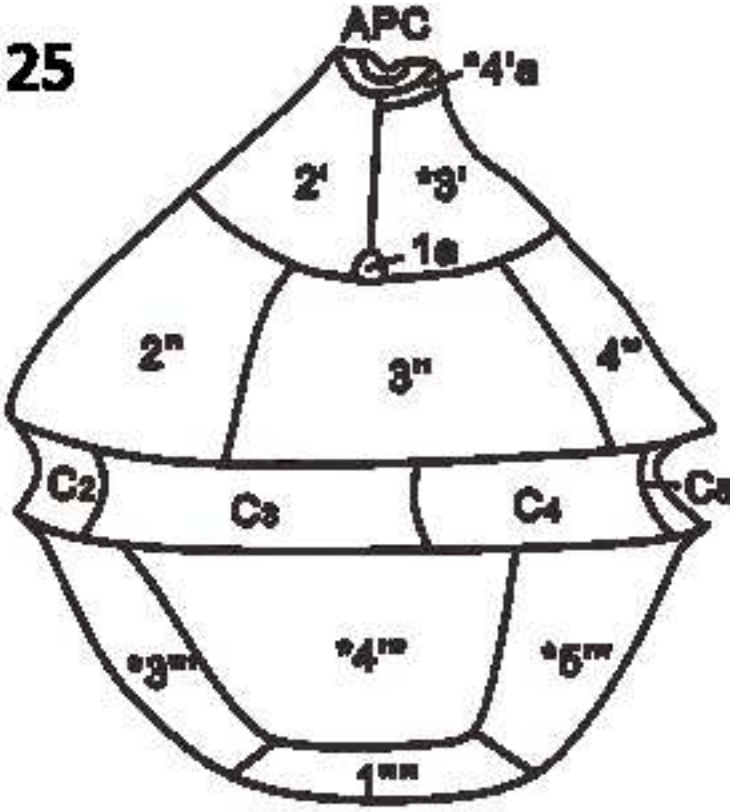

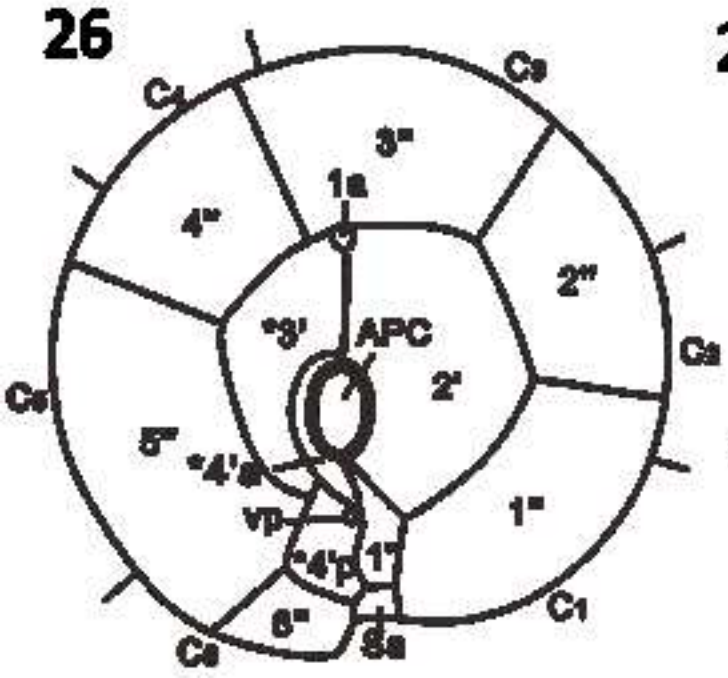

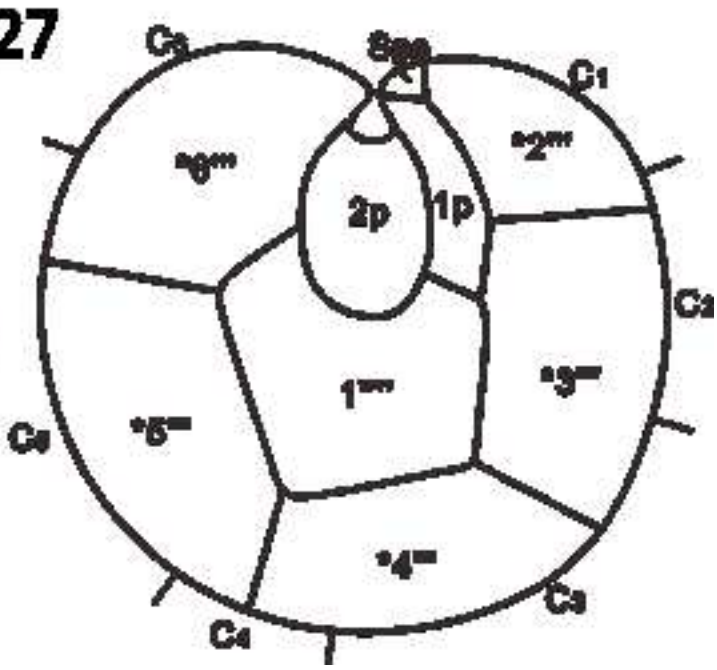

Figures 28-33

Click here to access/download;Figure;Fig. 28-33.tif

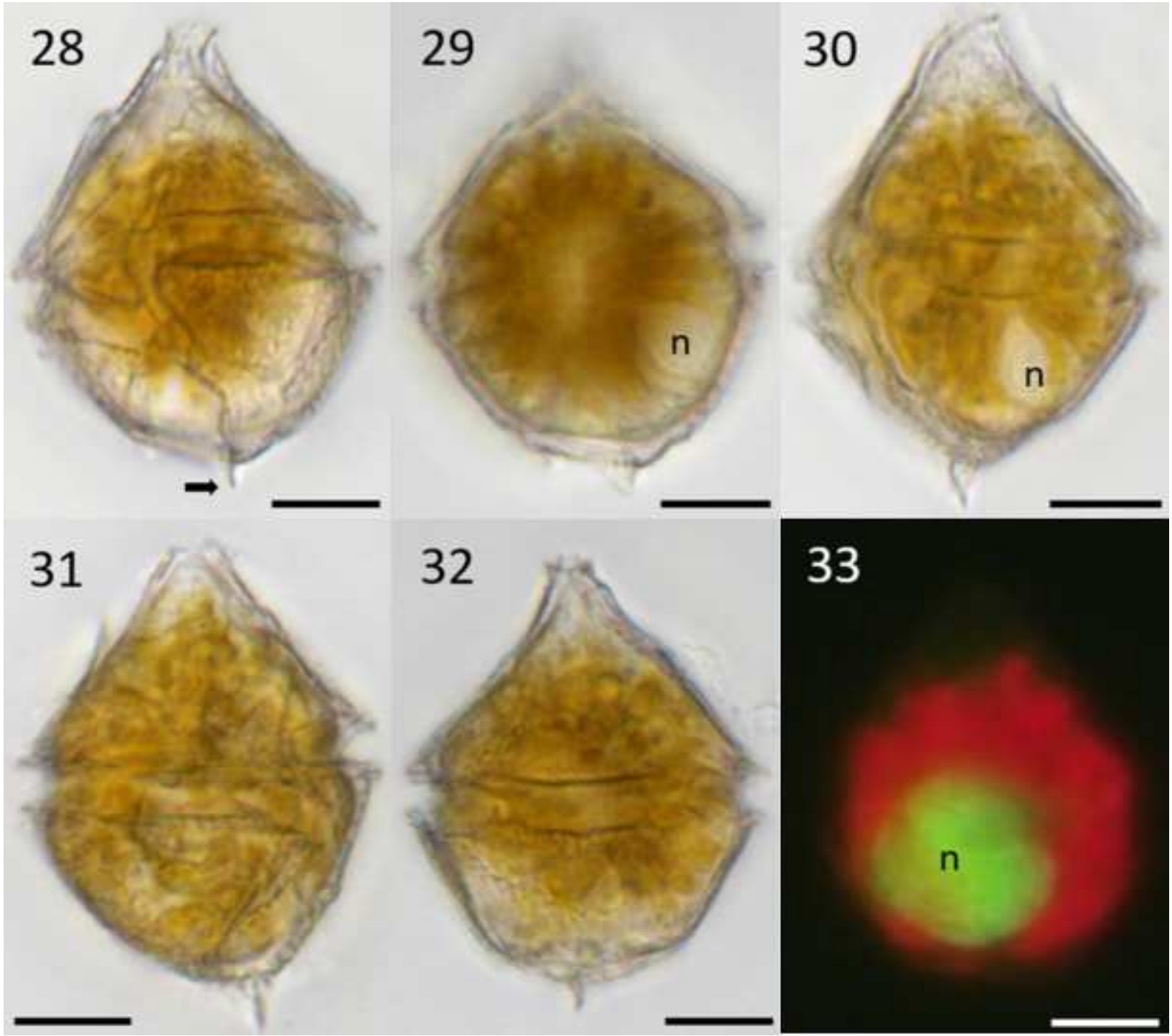

Figures 34-49

Click here to access/download;Figure;Fig. 34-49.tif

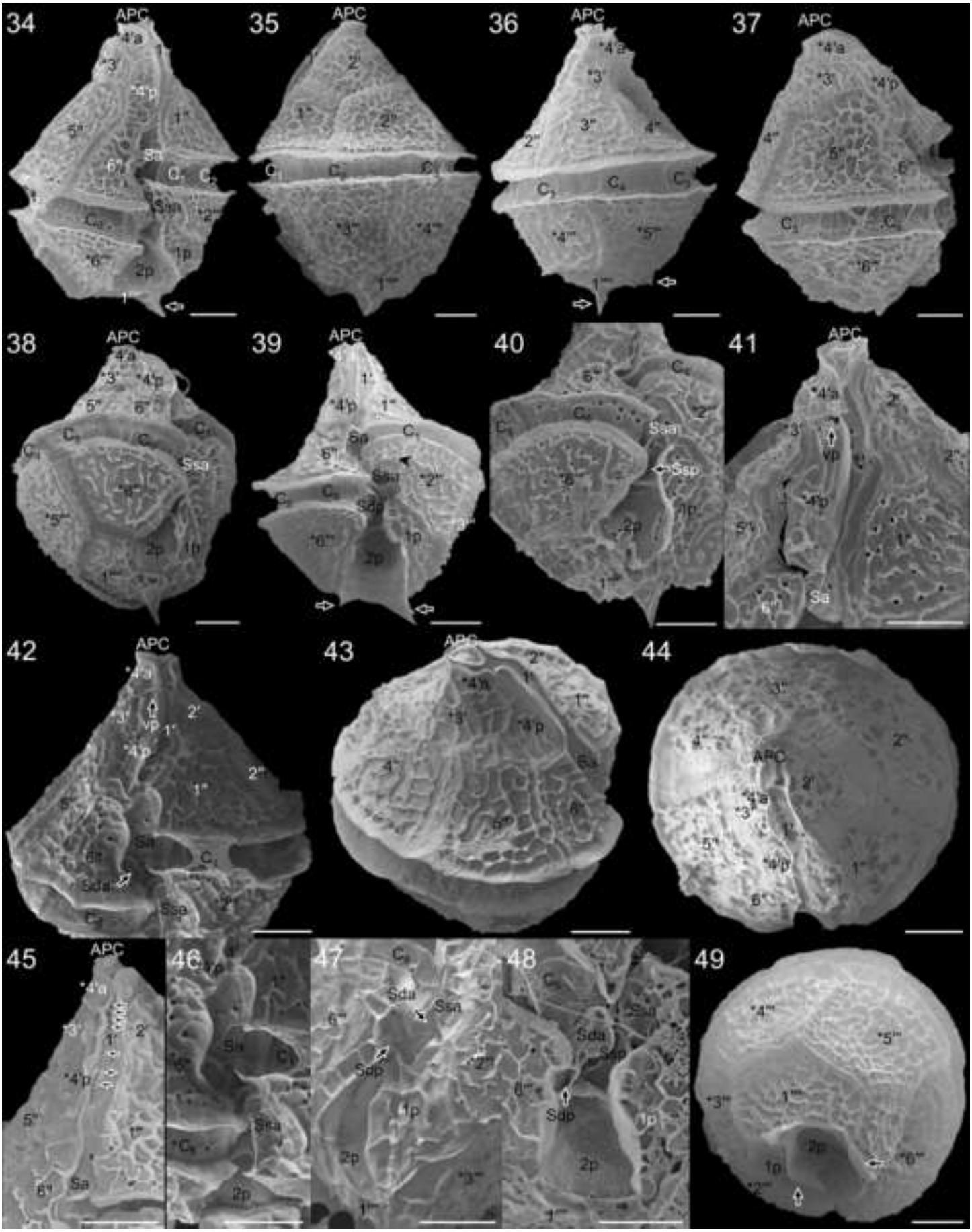

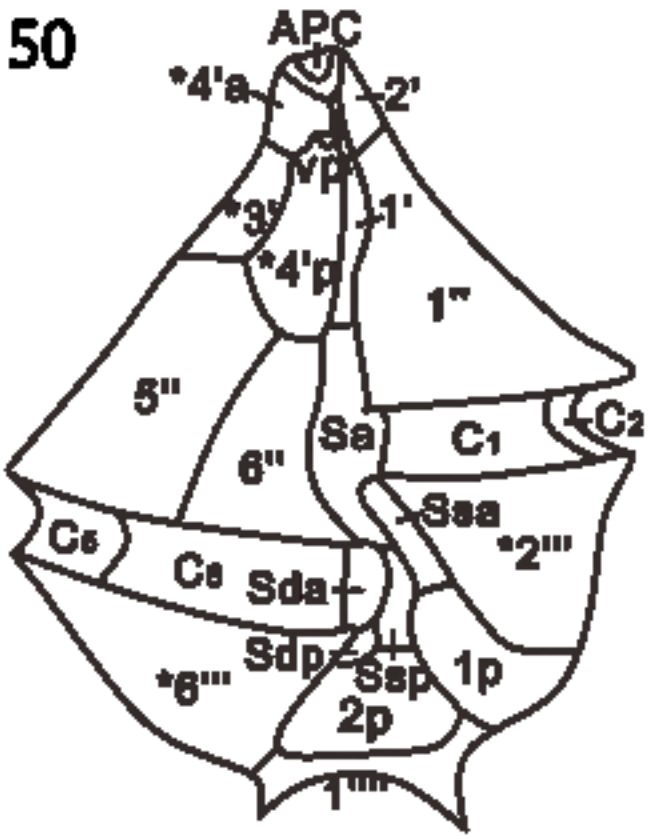

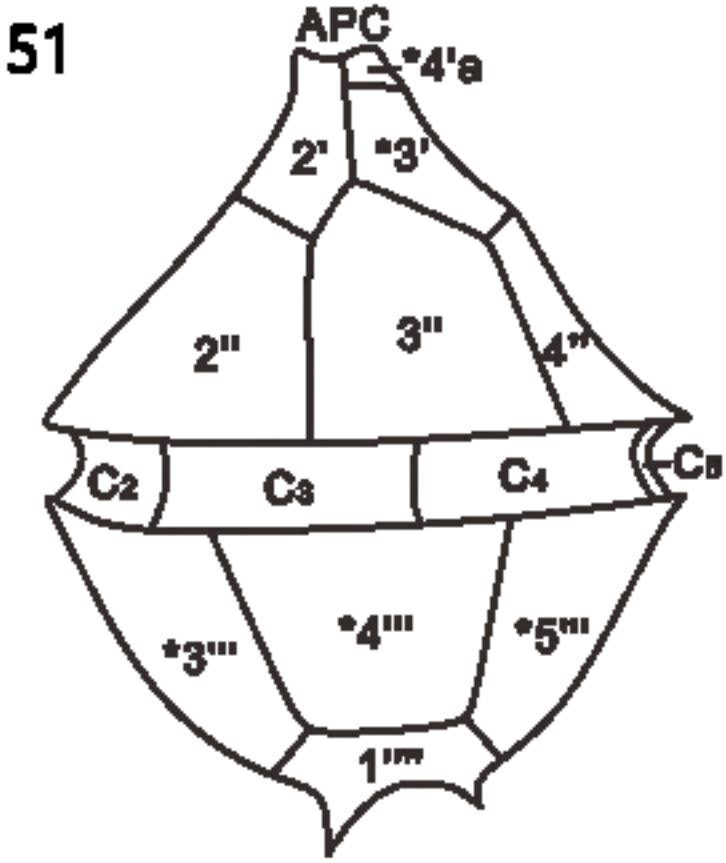

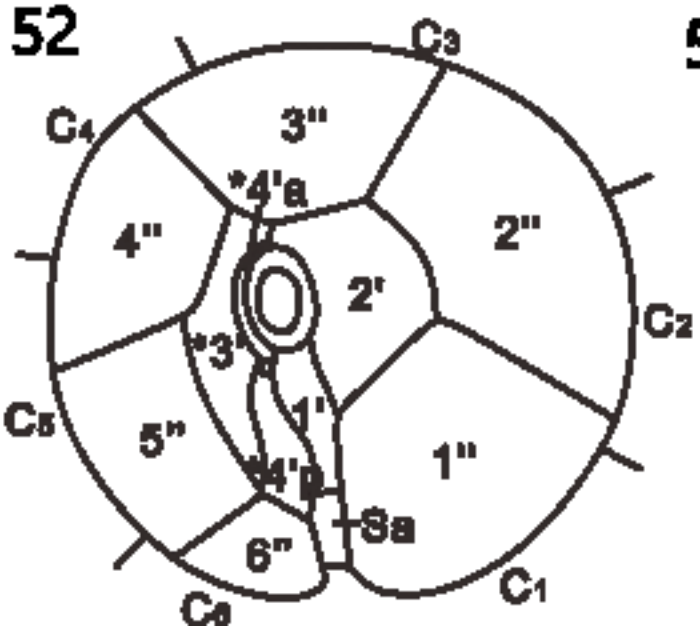

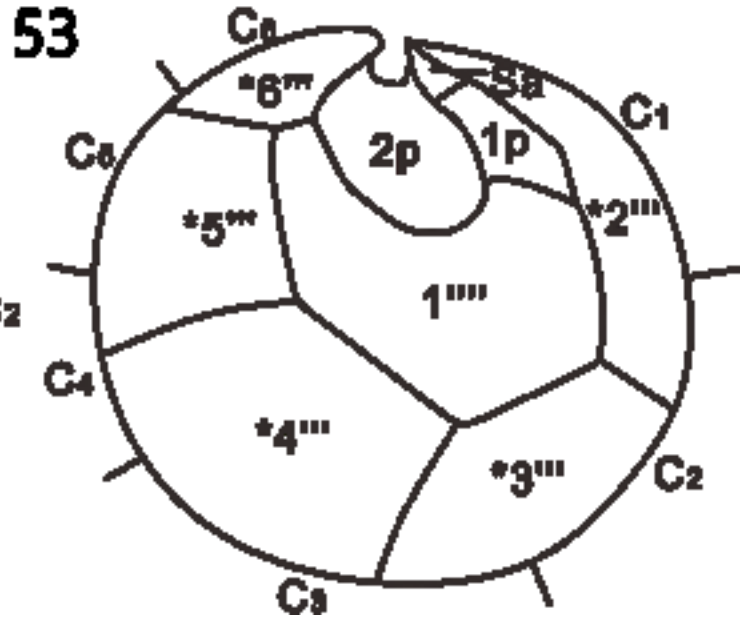

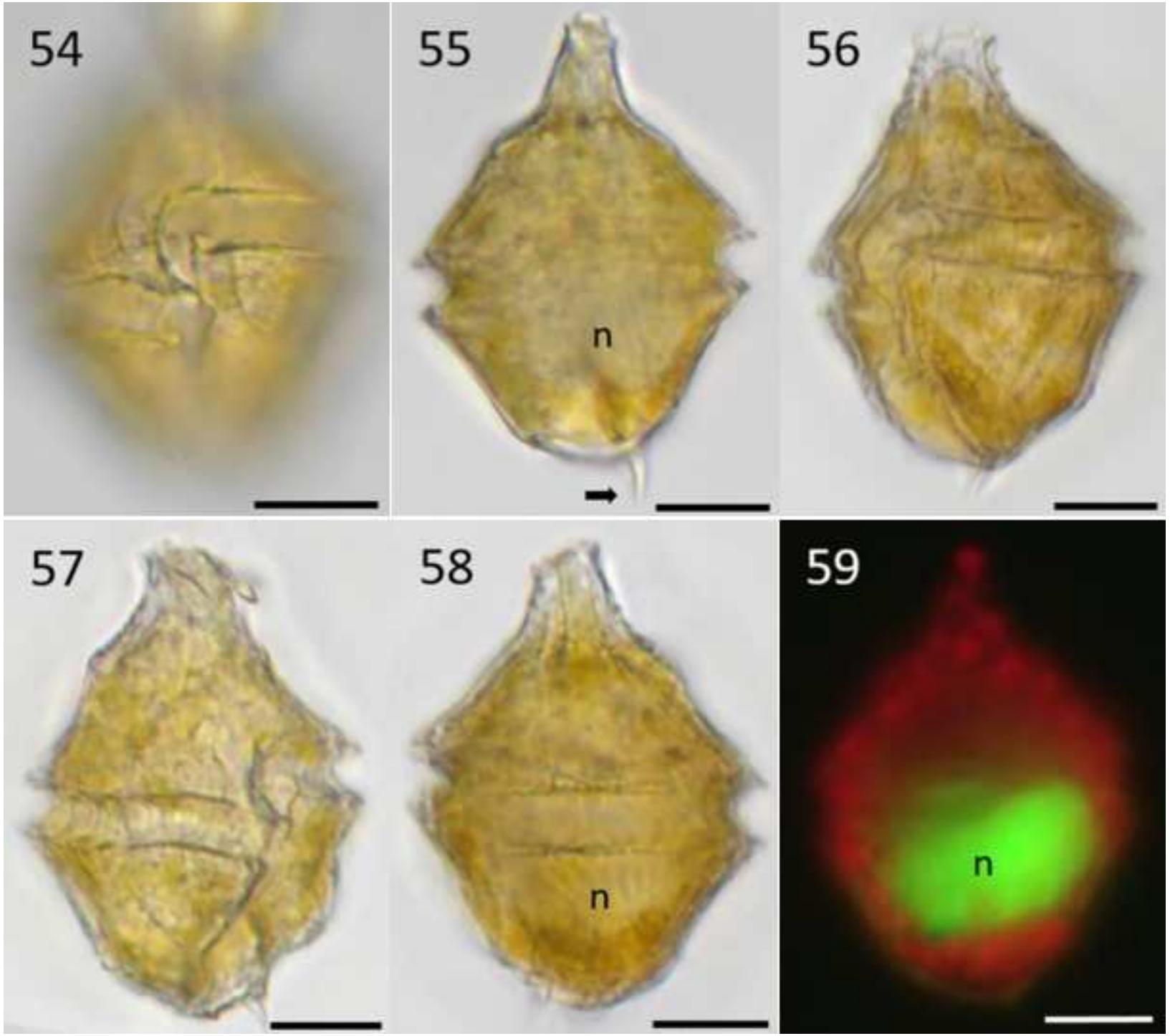

Figures 60-65

Click here to access/download;Figure;Fig. 60-65.tif

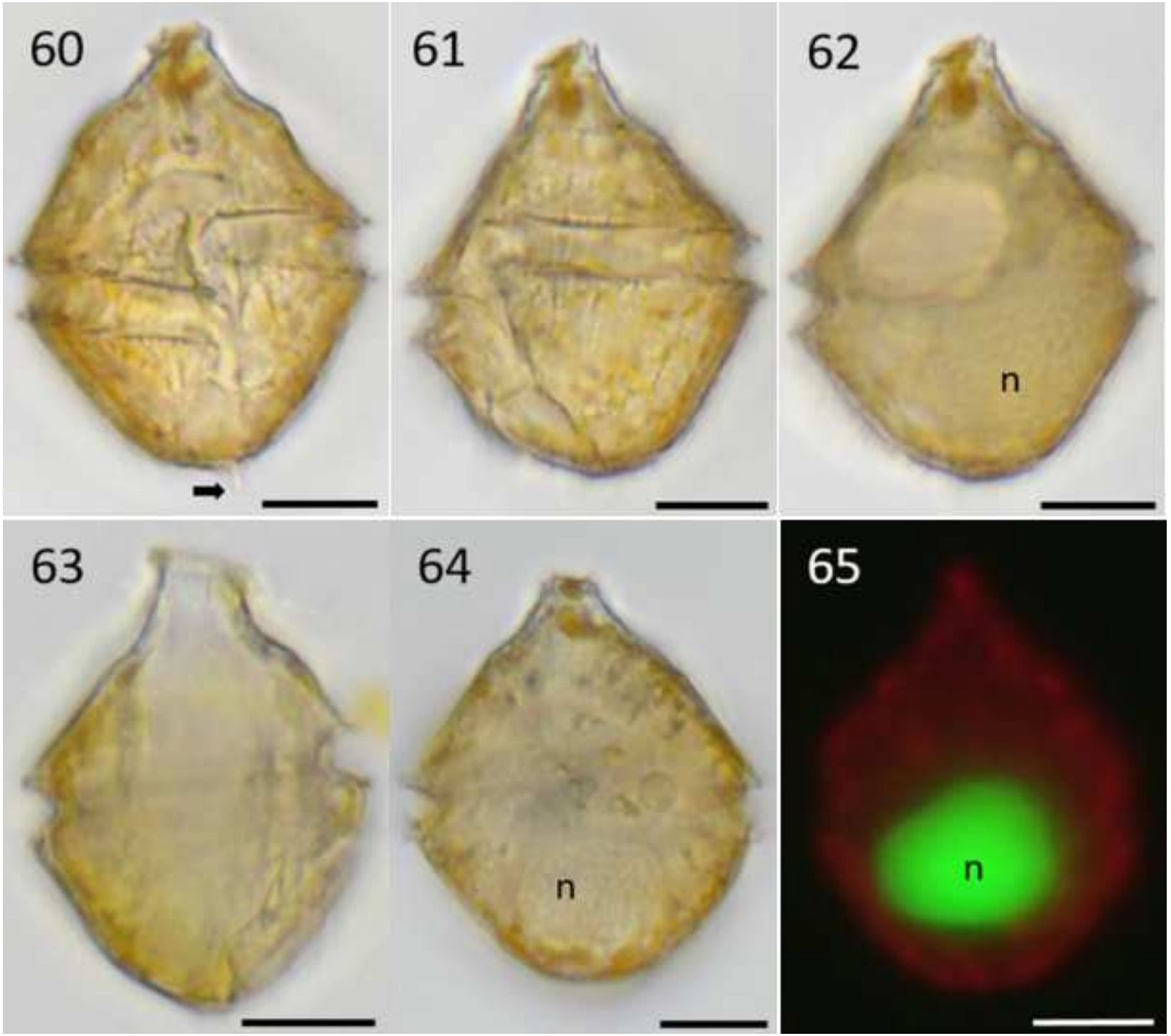

Figures 66-78

Click here to access/download;Figure;Fig. 66-78.tif

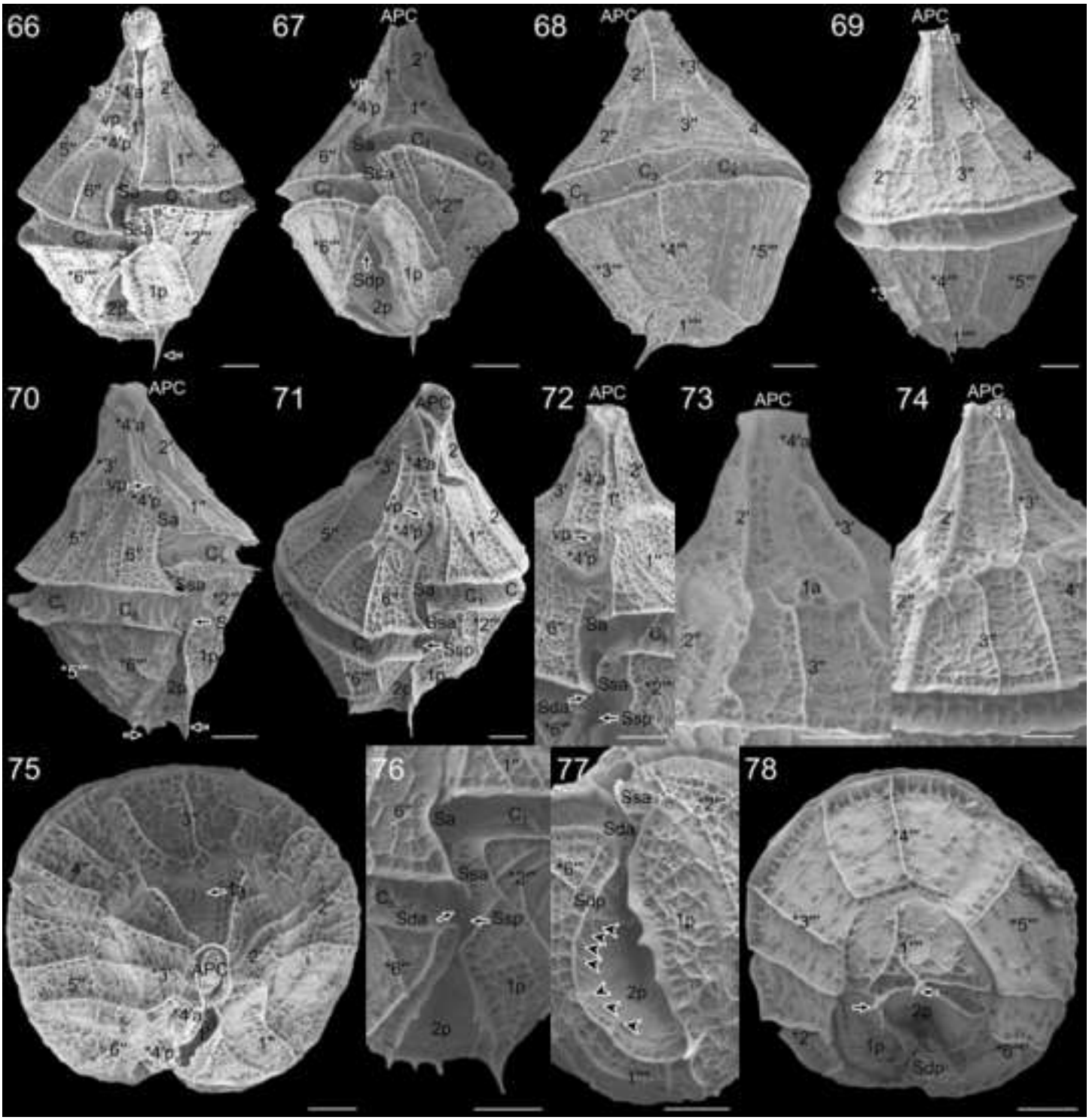

Figures 79-90

Click here to access/download;Figure;Fig. 79-90.tif

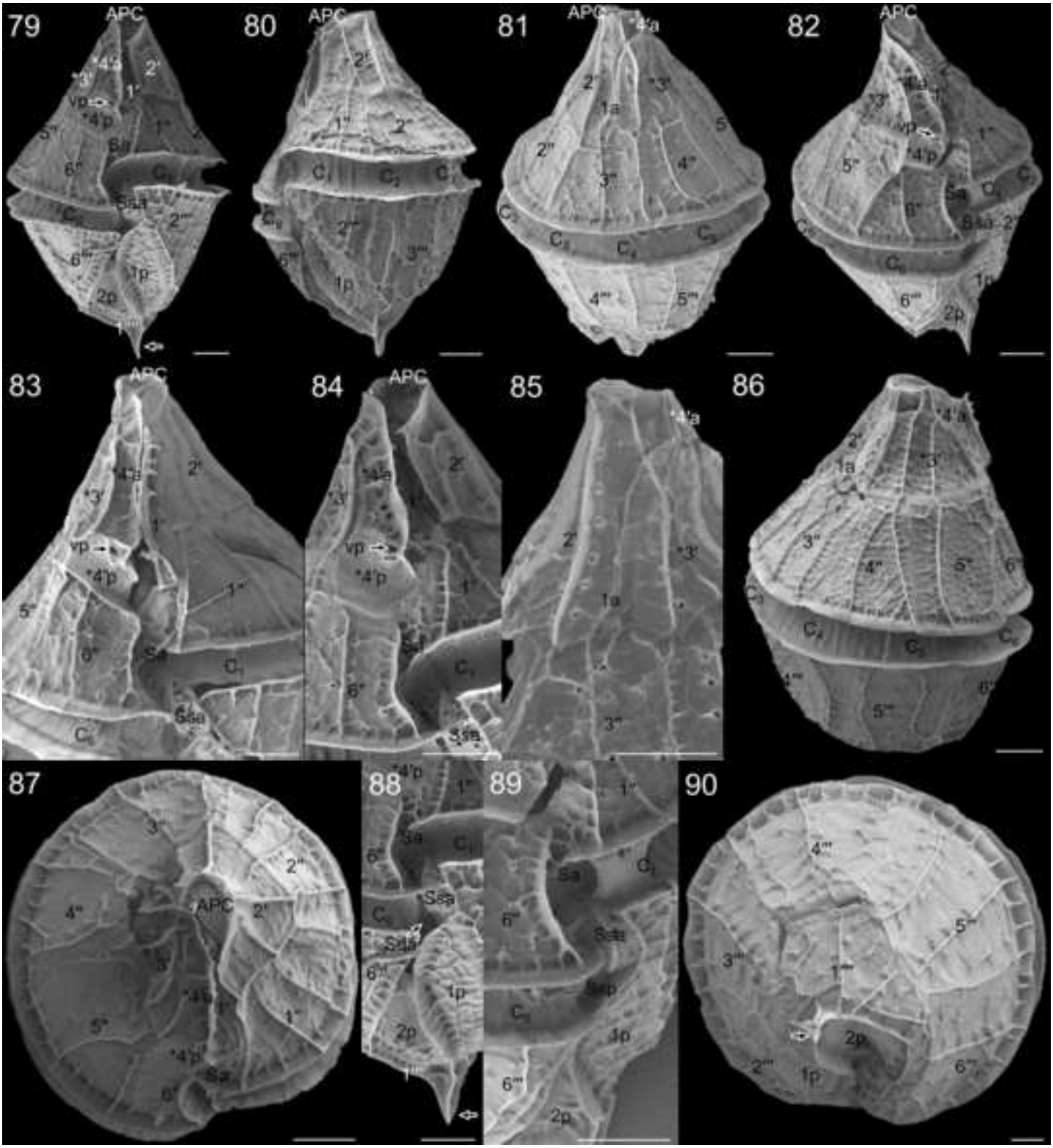

Click here to access/download;Figure;Fig. 91-98.tif

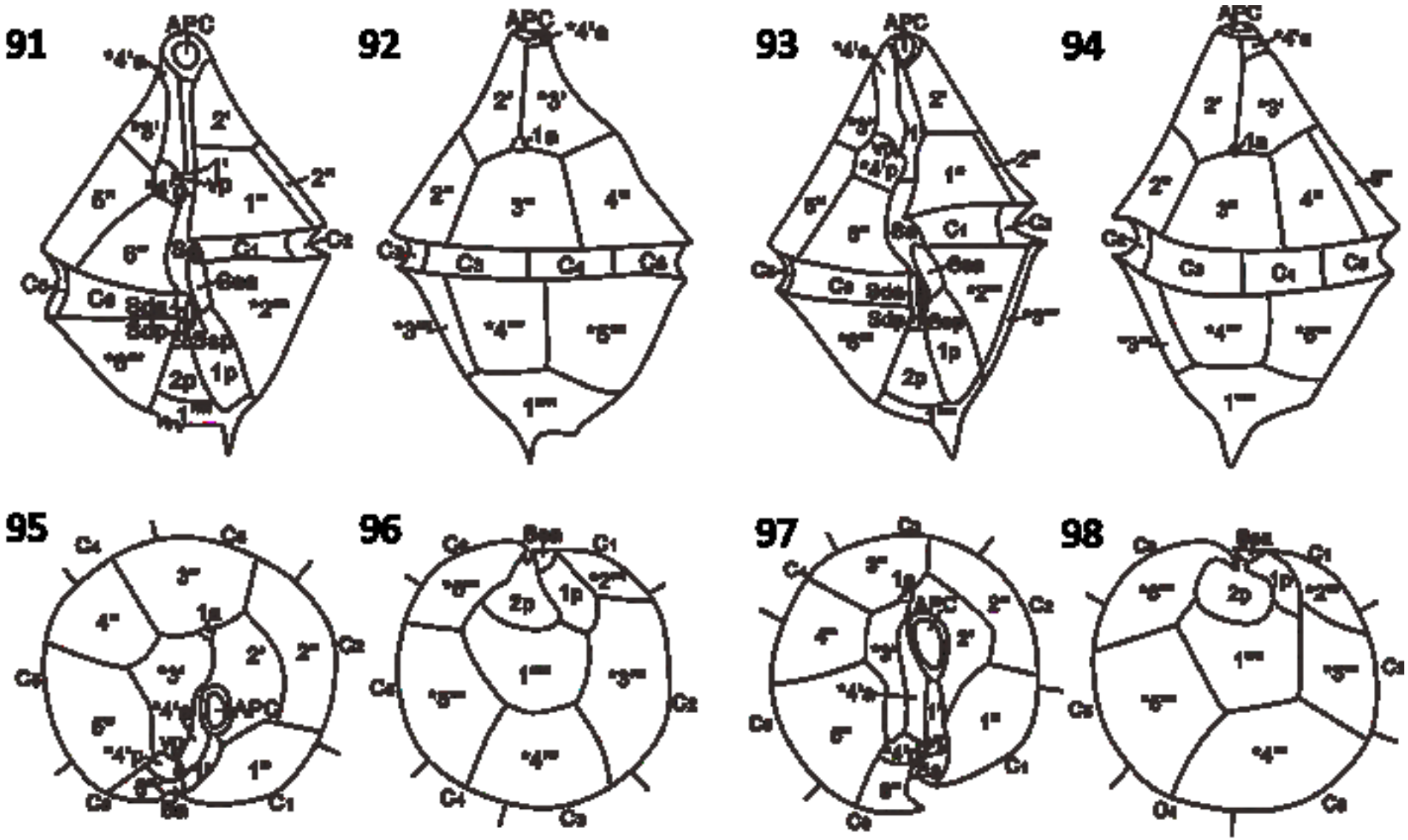

***Gonyaulax polygramma* ribotype 1** ***Gonyaulax polygramma* ribotype 2**

Fig_99_SHIN

Click here to access/download;Figure;Fig_99_SHIN.tif

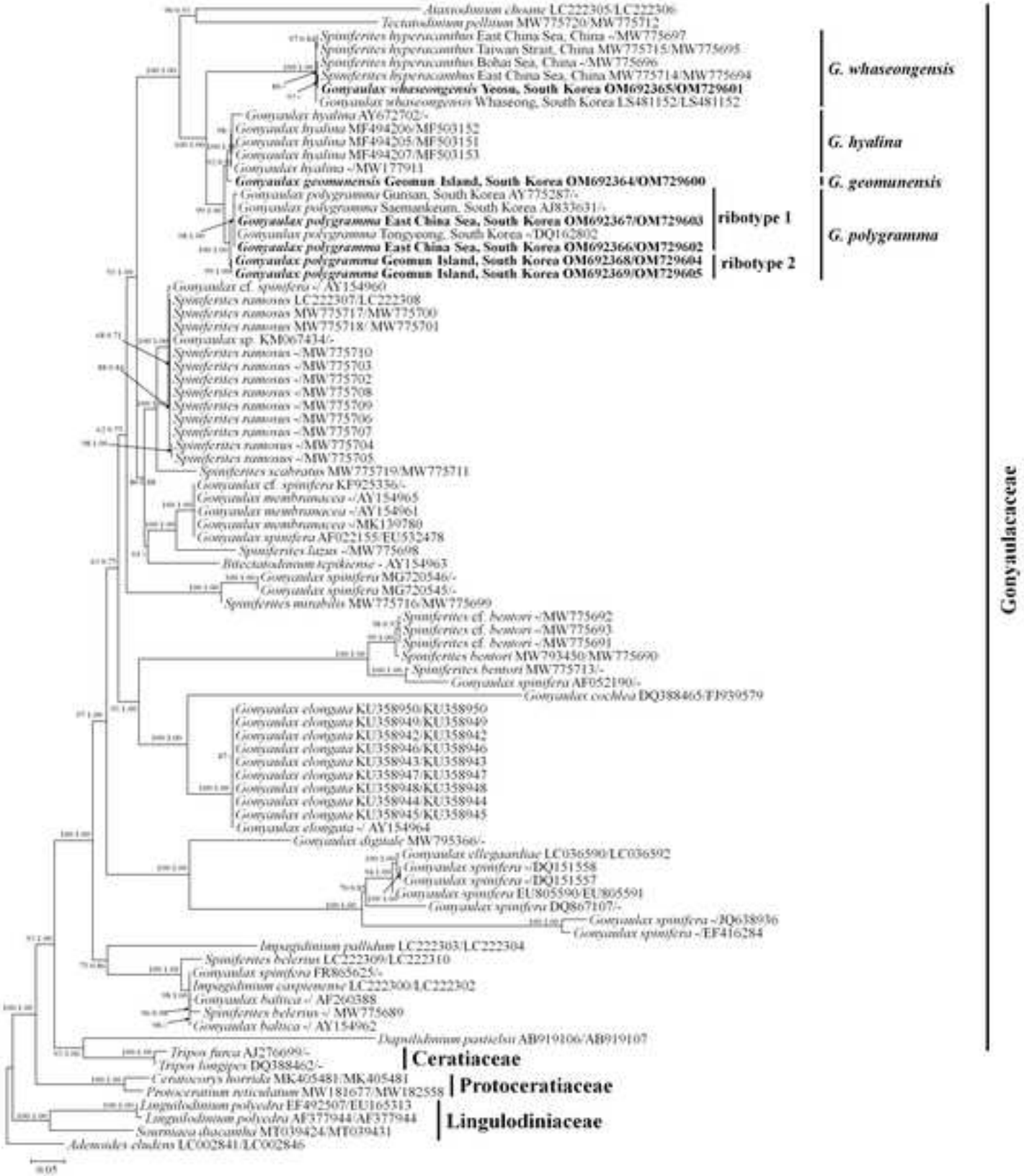

Figures 100-103

Click here to access/download;Figure;Fig. 100-103.tif